Neoplasia 62 (2025) 101143

Contents lists available at ScienceDirect

Neoplasia

journal homepage: www.elsevier.com/locate/neo

Original Research

Fatty acid synthase (FASN) inhibition cooperates with BH3 mimetic drugs to overcome resistance to mitochondrial apoptosis in pancreatic cancer

Travis Vander Steen [a], Ingrid Espinoza [b,c], Cristina Duran [d], Guillem Casadevall [d], Eila Serrano-Hervás [e,f], Elisabet Cuyàs [e,f], Sara Verdura [e,f], George Kemble [g], Scott H. Kaufmann [h,i,j], Robert McWilliams [h,i], Sílvia Osuna [d,k], Daniel D. Billadeau [h,j,l,m], Javier A. Menendez [e,f,**], Ruth Lupu [a,h,l,*]

[a] Division of Experimental Pathology, Department of Laboratory Medicine and Pathology, Mayo Clinic, Rochester, MN 55905, USA
[b] National Institute of Health, National Heart Lung and Blood Institute (NHLBI), Bethesda, MD 20817, USA
[c] Lung Development and Pediatric Branch (HNH36), Bethesda, MD 20817, USA
[d] Institut de Química Computacional i Catàlisi and Departament de Química, Universitat de Girona, Girona 17003, Spain
[e] Program Against Cancer Therapeutic Resistance (ProCURE), Catalan Institute of Oncology, Girona 17007, Spain
[f] Metabolism and Cancer Group,Girona Biomedical Research Institute (IDIBGI), Salt 17190, Girona, Spain
[g] Sagimet Biosciences Inc., San Mateo, CA 94402, USA
[h] Mayo Clinic Cancer Center, Rochester, MN 55905, USA
[i] Department of Molecular Pharmacology and Experimental Therapeutics, Mayo Clinic, Rochester, MN, 55905, USA
[j] Division of Oncology Research, Mayo Clinic, Rochester, MN, 55905, USA
[k] ICREA, Barcelona 08010, Spain
[l] Department of Biochemistry and Molecular Biology, Mayo Clinic, Rochester, MN 55905, USA
[m] Department of Immunology College of Medicine, Mayo Clinic, Rochester, MN 55905, USA

ARTICLE INFO

Keywords:
Pancreatic cancer
Fatty acid synthase
BH3 mimetics
Gemcitabine

ABSTRACT

Resistance to mitochondrial apoptosis is a major driver of chemoresistance in pancreatic ductal adenocarcinoma (PDAC). However, pharmacological manipulation of the mitochondrial apoptosis threshold in PDAC cells remains an unmet therapeutic goal. We hypothesized that fatty acid synthase inhibitors (FASNis), a family of targeted metabolic therapeutics recently entering the clinic, could lower the apoptotic threshold in chemoresistant PDAC cells and be synergistic with BH3 mimetics that neutralize anti-apoptotic proteins. Computational studies with TVB-3166 and TVB-3664, two analogues of the clinical-grade FASNi TVB-2640 (denifanstat), confirmed their uncompetitive behavior towards NADPH when bound to the FASN ketoacyl reductase domain. The extent of NADPH accumulation, a consequence of FASN inhibition, paralleled the sensitivity of PDAC cells to the apoptotic effects of TVB FASNis in conventional PDAC cell lines that naturally express varying levels of FASN. FASN inhibition dramatically increased the sensitivity of "FASN-high" expressing PDAC cells to the BCL2/BCL-X_L/BCL-W inhibitor ABT-263/navitoclax and the BCL2-selective inhibitor ABT-199/venetoclax, both *in vitro* and in *in vivo* xenografted tumors. The ability of TVB FASNis to shift the balance of pro- and anti-apoptotic proteins and thereby push PDAC cells closer to the apoptotic threshold was also observed in cell lines developed from patient-derived xenografts (PDXs) representative of the classical (pancreatic) transcriptomic subtype of PDAC. Experiments in PDAC PDXs *in vivo* confirmed the synergistic antitumor activity of TVB-3664 with navitoclax and venetoclax, independent of the nature of the replication stress signature of patient-derived PDAC cells. The discovery that targeted inhibition of FASN is a metabolic perturbation that sensitizes PDAC cells to BH3 mimetics warrants further investigation to overcome resistance to mitochondrial apoptosis in PDAC patients.

* Corresponding author at: 200 First Street SW, Rochester, Minnesota 55905, USA, Biochemistry and Molecular Biology, Experimental Pathology and Medicine, Mayo Clinic College of Medicine, Mayo Clinic Cancer Center.
** Corresponding author at: Edifici M2, Parc Hospitalari Martí i Julià, E-17190, Salt (Girona), Spain, Program Against Cancer Therapeutic Resistance (ProCURE), Catalan Institute of Oncology (ICO), Girona Biomedical Research Institute.
E-mail addresses: jmenendez@idibgi.org (J.A. Menendez), Lupu.ruth@Mayo.edu (R. Lupu).

https://doi.org/10.1016/j.neo.2025.101143
Received 5 September 2024; Accepted 17 February 2025

Introduction

Pancreatic ductal adenocarcinoma (PDAC) is the fourth leading cause of cancer-related mortality worldwide and is projected to become the second deadliest solid tumor by 2030 [1]. Despite small improvements in the survival rate for the subset of patients who undergo surgical resection [2–4], the 5-year survival rate for PDAC remains approximately 5 % [5]. The nucleoside analog gemcitabine, which has been widely used for the treatment of PDAC across all stages of the disease, exhibits suboptimal clinical activity with frequent development of chemoresistance within weeks of treatment initiation [6–9]. Chemotherapy regimens such as the FOLFIRINOX protocol (fluorouracil, leucovorin, irinotecan, and oxaliplatin [10]), the combination of gemcitabine plus nab-paclitaxel [11], or a modified FOLFIRINOX regimen containing gemcitabine [12] have slightly improved survival rates in the treatment of metastatic PDAC, but their clinical efficacy remains unsatisfactory and at the expense of a higher incidence of toxic effects. To improve the dismal prognosis of PDAC, therapeutic agents with novel mechanisms of action are urgently needed to be combined with current standard chemotherapy.

The inherent or rapidly acquired resistance of PDAC not only to conventional radiotherapy and chemotherapy, but also to new targeted therapies, is largely due to concerted molecular alterations that disrupt mitochondrial apoptosis-inducing signals and counteract the execution of mitochondrial apoptosis in PDAC cells [5,13–16]. Indeed, the imbalance between anti-apoptotic and pro-apoptotic Bcl-2 family members commonly observed in PDAC has been associated with resistance to chemotherapy [17–20]. Thus, functional restoration of the mitochondrial apoptosis pathway using small molecule inhibitors called BH3 mimetics may represent a valuable strategy to overcome the therapeutic refractoriness of PDAC [21]. BH3 mimetics mechanistically act as competitive inhibitors that occupy the BH3-binding hydrophobic groove of anti-apoptotic BCL-2 proteins (e.g., BCL-2, BCL-X_L, MCL-1), thereby interfering with their functional ability to sequester the pro-apoptotic, BH3-only BCL-2 family members (e.g., BIM, BID, BAD, PUMA, and NOXA), which ultimately trigger the mitochondrial apoptotic pathway by inducing the homo-oligomerization of BAX/BAK effectors [22–27]. As monotherapy, BH3 mimetics increase the apparent stoichiometry of pro-apoptotic BH3-only proteins and show promising activity in hematological malignancies but have been largely ineffective in solid tumors such as PDAC. There is increasing evidence that the ability of BH3 mimetics to induce apoptotic cell death depends on the so-called “mitochondrial priming” or how close a cell is to the threshold of mitochondrial apoptosis [28–33]. In addition, the level of mitochondrial priming has been shown to correlate strongly with increased chemosensitivity and clinical response in several cancers [34–36]. Thus, the true therapeutic potential of directly targeting the mitochondrial pathway of apoptosis in PDAC may be unlocked by new drugs capable of promoting a high mitochondrial primed-for-death state.

Fatty acid synthase (FASN) –the only enzyme capable of catalyzing the *de novo* biosynthesis of endogenous FAs from simple metabolic precursors [37]– is a lipogenic hallmark of cancer metabolism that has been associated with poor prognosis in cancer patients [38–42]. Previous studies have shown that FASN overexpression in tumor tissue, as well as elevated levels of circulating serum FASN, could be used as biomarkers of biological aggressiveness, recurrence risk and shortened survival in PDAC patients [43–45]. FASN activation also appears to confer a significant survival advantage to PDAC cells in response to gemcitabine [46–48]. This suggests that pharmacological ablation of FASN-driven endogenous lipogenesis may be an innovative approach to overcome the intrinsic chemoresistant phenotype of PDAC tumor cells. However, most of the preclinical evidence demonstrating significant increases in gemcitabine sensitivity by blocking FASN activity has used short hairpin RNA gene silencing or first-generation FASN inhibitors (FASNis) with very limited clinical relevance. While testing the mechanistic aspects of the so-called TVB series of clinical-grade FASNis, which are now being studied in various phase II trials [42,49–51], we have recently identified FASN as an unexpected metabolic regulator of mitochondrial apoptotic priming in breast cancer cells [52]. FASNis reorganized the interactome of the BCL-2 network to place breast cancer cells in a higher state of death readiness that was exquisitely dependent on certain anti-apoptotic proteins to sequester pro-apoptotic BH3-only proteins. BCL-2-targeted BH3 mimetics were found to fully unleash the intrinsic apoptotic pathway in FASN-inhibited, primed-for-death breast cancer cells [42,52]. Whether this mechanism of action of FASNis is unique to breast cancer or is a common pan-cancer feature that could be exploited for therapeutic purposes remains to be determined.

Here, to develop a unique mitochondrial apoptosis-centered therapeutic strategy for PDAC, we hypothesized that targeted inhibition of FASN may be able to lower the apoptotic threshold in PDAC cells to synergize with pro-apoptotic BH3 mimetics. Using close analogues of the clinical FASNi TVB-2640 (denifanstat), conventional PDAC cell lines, and cell lines developed from patient-derived xenografts (PDXs) *in vitro* and *in vivo*, we now demonstrate that FASN is a metabolic vulnerability that can be therapeutically exploited to sensitize PDAC to BH3 mimetics.

Materials and methods

Reagents

TVB-3664 was provided by 3V-Biosciences/Sagimet Biosciences (San Mateo, CA). Other reagents were purchased from the following suppliers: C75 (#2489) from Tocris Bioscience (Minneapolis, MN); ABT-263/navitoclax (#A3007) from APExBio (Houston, TX); ABT-199/venetoclax (#CT-A199) from ChemieTek (Indianapolis, IN); TVB-3166 (#SML1694), NAC, and anti-β-actin (#A2228) antibody from Sigma-Aldrich (St. Louis, MO); allophycocyanin (APC)-conjugated annexin V and binding buffer from BD Biosciences (San Diego, CA); anti-BIM (#2819), anti-BCL-X_L (#2764), anti-MCL-1 (#4572), and anti-BAX (#2772) antibodies from Cell Signaling Technology Inc. (Danvers, MA) and Fisher Healthcare (Waltham, MA), respectively; anti-PUMA (#SC-374223) from Santa Cruz Biotechnology, Inc. (Dallas, TX); anti-BAK (#06-536) from Merck Millipore (Burlington, MA); anti-BCL2 (#M0887) from Dako (Carpinteria, CA); anti-NOXA (#ALX-804-408-C100) was from Enzo Life Sciences (Farmingdale, NY); InnoCyte™ Flow Cytometry Cytochrome c Release Kit from Calbiochem (Los Angeles, CA); Carboxy-H_2DCFDA and Superscript III First Strand Synthesis from Life Technologies (Carlsbad, CA). MTT from Promega (Madison, WI); Supersignal West Pico chemiluminescent reagent and BCA protein assay from Pierce (Rockford, IL); RNeasy kits from Qiagen (Hilden, Germany); Phosal 50 from Medchem Express (Manmouth Junction, NJ); IMEM, DMEM/F12, and L-glutamine from Gibco (Waltham, MA); and $NADP^+$/NADPH Quantification kit from BioVision (Mountain View, CA).

Drug complexing/formulation

Palmitate (#P9767, Sigma-Aldrich) was complexed with BSA. Briefly, palmitate was dissolved in ethanol to 150 mmol/L, diluted 1:5 in a 4 % (w/v) BSA solution in 0.9 % NaCl and incubated for 1 h at 37 °C to obtain a 30 mmol/L stock of BSA-complexed palmitate. TVB-3664 was dissolved in 100 % PEG-400 and diluted with water to a final PEG concentration of 30 % immediately prior to oral gavage. ABT-263 and ABT-199 were reconstituted in 10 % ethanol, 30 % PEG400, and 60 % Phosal 50 for oral gavage.

Cell lines

Established PDAC cell lines PANC-1, MIA Paca-2, and BxPC-3, as well as cells isolated from pancreatic cancer patient-derived xenografts (4666, 5160, 6052, 4911, 4833, 5641, 6105, 4535, 6164, and 4041) were used in this study. PANC-1 (CRL-1469), MIA Paca-2 (CRL-1420),

and BxPC-3 (CRL-1687) were purchased from ATCC (Manassas, VA, USA). PDX-derived PDAC cell lines were provided by the Pancreatic Cancer SPORE Tissue and Cell repository (Mayo Clinic, Minnesota). The procedure for isolation of these cells from PDAC-derived xenografts has been described elsewhere [82,83,85,86,105]. PANC-1, MIA Paca-2, and BxPC-3 cells were routinely expanded in Improved Minimum Essential Medium (IMEM, Gibco, Waltham, MA) supplemented with 10 % heat-inactivated fetal bovine serum (FBS), 1 % L-glutamine, 1 % sodium pyruvate, 1 % penicillin-streptomycin. BxPC-3 cells were maintained in RPMI1640 medium supplemented with 10 % FBS and 1 % L-glutamine (Gibco, Waltham, MA). PDX-derived PDAC cell lines were cultured in DMEM/F12 medium supplemented with 10 % FBS and 1 % L-glutamine (Gibco, Waltham, MA).

Cells were grown at 37 °C in a humidified atmosphere containing 5 % CO_2. Cells grown to 70–80 % confluence were used at the beginning of all the experiments. Cell lines were authenticated by STR profiling, both performed by the manufacturer and confirmed in-house at the time of purchase according to ATCC guidelines. Cells were passaged by starting a low-passage cell stock every month until to 2–3 months after resuscitation. Cell lines were screened for mycoplasma contamination using a MycoAlert Mycoplasma Detection ELISA (Lonza, Basel Tower, Switzerland) prior to experimentation and were intermittently tested thereafter.

In silico modeling of human FASN

Cryo-EM structures of the core modifying region of human FASN have recently been deposited in the Protein Data Bank (PDB) under the accession numbers 8EYI (NADPH bound), 8EYK, and 8GKC (NADPH + TVB2640 FASNi bound) [66]. In this study, we used the AlphaFold2 (AF2) neural network [106] to build a complete model of the core modifying region, including the ACP domain according to UniProtKB P49327 entry, using an extended FASTA sequence from the 8EYK structure as input. To obtain different conformations of the FASN active site, some modifications were made to the AF2 settings, including the use of a single template from the available PDBs 8EYK and 4PIV, and only the parameters from the model_2_ptm with the reduction of the max_extra_msa to 256 and max_msa_clusters to 128. To reduce the computational complexity of the docking step, the AF2 models were reduced to a compact Psi/KR tri-domain structure. This structure is composed of the keto-reductase (KR) catalytic domain (1864–2118) and the two catalytically incompetent pseudo-KR (ΨKR) (1392–1521) and pseudo-methyltransferase (ΨME) (1109–1391) domains, which are close in space to KR. To obtain these reduced models, the ER catalytic domain (1635–1863), as well as the DH domain (838–1108), and the ACP motif (2121–2198) were removed according to the UniProtKB P49327 numbering.

Molecular docking assays

The *known-pocket* docking program HADDOCK3 (HADDOCK3, Bonvin's Lab, https://github.com/haddocking/haddock3, [107,108]) was used to find the correct orientation and conformation of TVB FASNis in the selected binding pocket of FASN. We used the compact model of the Psi/KR tri-domain including the bound NADPH cofactor using PyMOL software (PyMOL Molecular Graphics System, Version 2.0 Schrödinger, LLC (n.d.), retrieved May 15, 2023 from https://pymol-org/2/support.html?). The NADPH parameters were obtained from http://amber.manchester.ac.uk/cof/nad_ryde_inf.html. The structures of TVB-2640, TVB-3166, TVB-3664 and GSK-2194069 molecules were obtained directly from the PubChem database and optimized using Gaussian 16 a03 (Gaussian 16) at the DFT level (B3LYP/6-311G (d, p) level of theory and including GD3BJ empirical dispersion [109]. Partial charges of each molecule were obtained using PyRESP (Python Restrained Electrostatic Potential) program [110] to apply the Restrained Electrostatic Potential (REsP) fitting approach using the electrostatic potential generated at the HF/6-31(d) level of theory. Topology and parameter files were obtained using the antechamber module of AMBER23 (https://ambermd.org/CiteAmber.php) and the ACPYPE (AnteChamber PYthon Parser interfacE) program [111]. Different tautomers for imidazole, pyrazole and triazole were also considered as shown in Fig. S2. For the HADDOCK3 docking calculations, the "rigidbody" parameters were set as follows: w_vdw to 0.01, w_elec to 1.0, epsilon to 10, inter_rigid to 0.001. For the "flexref" parameters, we configured w_vdw to 1.0, w_elec to 0.1, epsilon to 1, with mdsteps_rigid and mdsteps_cool1 set to 0, and initial temperatures set at temp_cool2_init to 500 and temp_cool3_init to 300. Under this strategy, 56 active site residues at the catalytic core of the KR domain were considered. The obtained docking poses for each inhibitor were ranked according to the quality indicative HADDOCK score, but selected binding poses were also finally selected by careful visual inspection.

Annexin V binding by flow cytometry

Binding of allophycocyanin (APC)-conjugated annexin V to cells was assessed by flow cytometry. Briefly, cells were plated at 3×10^5 cells/well in a 6-well plate and allowed to adhere overnight before replacing the culture medium with fresh medium containing different concentrations of FASN inhibitors and/or BH3 mimetics. After 48 h of treatment, both adherent and floating cells were collected, washed with PBS and suspended in 100 µL of annexin binding buffer consisting of 140 mM NaCl, 2.5 mM $CaCl_2$, and 10 mM HEPES (pH 7.4). After the addition of 5 µL of APC-coupled Annexin V and incubation at room temperature (RT) for 15 min, cells were stained with 400 µL annexin binding buffer containing 0.1 µg/mL propidium iodide and immediately subjected to flow cytometry. A total of 20,000 events were collected from the FL3 (excitation 488 nm, emission 650 LP) and FL4 (excitation 635 nm, emission 661 ± 8 nm) channels of a Becton Dickinson Accuri C6 flow cytometer, and data were analyzed using Accuri C6Flow software.

Cytochrome c release assay

Cytochrome c release was assayed using the InnoCyte™ Flow Cytometry Cytochrome c Release Kit (Calbiochem, Los Angeles, CA). Briefly, 1–3 × 10^6 cells were harvested and centrifuged at 1000 × *g* for 5 min. The pellet was gently resuspended in 300 µL of permeabilization buffer and incubated on ice for 10 min. Then, 300 µL of 8 % paraformaldehyde in PBS was added directly to the tubes to fix the cells. After gentle mixing by inverting the tubes 5 times, the cells were incubated at RT for 20 min and then collected by centrifugation at 1000 × *g* for 5 min. The pellet was washed three times with 1 mL of wash buffer, followed by centrifugation. Finally, the cells were gently resuspended in 250 µL of blocking buffer and incubated for 1 h at RT. After the blocking step, 250 µL of anti-cytochrome c working solution was added to each tube and gently mixed by inversion 5 times. After incubation for 1 h at RT, the cells were washed with wash buffer and 500 µL of FITC-conjugated anti-IgG working solution was added. The mixture was incubated for 1 h at RT in the dark, followed by a single wash with wash buffer. For flow cytometry, the cells were gently resuspended in 500 µL wash buffer, and for fluorescence microscopy the cell pellet was gently resuspended in 100 µL of wash buffer containing 1 µL of DAPI (100 µg/mL stock). After incubation for 10 min in the dark, a single drop of cell suspension was placed on a standard microscope slide and covered with a glass coverslip. Cells were observed on a Zeiss Axio Imager A1 using a 10 × dry objective.

Assessment of intracellular reactive oxygen species (ROS)

Intracellular ROS production was monitored using the permeable fluorescent dye 5-(and-6)-carboxy-2,7-dichlorodihydrofluorescein diacetate (carboxy-H_2DCFDA) (Invitrogen), which reacts predominantly with H_2O_2 and nitric oxide to form the fluorescent product 2,7-dichlorodihydrofluorescein (DCF), and dihydroethidine (DHE) (Sigma-

Aldrich), which is particularly sensitive to superoxide (O_2^-) and hydroxyl (OH·) radicals. For both probes, the intracellular fluorescence intensity is proportional to the amount of ROS generated by the cells. For carboxy-H_2DCFDA staining, cells were incubated with 50 μM carboxy-H_2DCFDA (dissolved in PBS) for 30 min after treatment. For HE staining, 5 μM HE was added to the cultured cells 30 min before the end of the treatment. After two washes with PBS, cells were harvested, resuspended in PBS and adjusted to a density of 10^6 cells/mL. Fluorescence intensity of intracellular DCF (excitation 488 nm, emission 530 nm) or ethidium (excitation 488 nm, emission 585 nm) was measured by flow cytometry. A total of 10^4 events were counted and the data were analyzed using Accuri C6 Flow software.

Determination of the NADPH/NADP$^+$ ratio

The NADPH/NADP$^+$ ratio was determined using a NADP$^+$/NADPH quantification kit (BioVision, Mountain View, CA) with minor modifications. After treatment, cells were washed with cold PBS and 1.5×10^6 cells for each assay were collected in a microcentrifuge tube (2000 rpm, 5 min). Cells were extracted with 300 μL of NADP/NADPH Extraction Buffer by two freeze/thaw cycles (20 min on dry ice, followed by 10 min at RT), mixed for 10 s, and centrifuged at 14000 rpm for 5 min. The supernatant was transferred to two new tubes (150 μL/per tube). For the detection of total NADP/NADPH (NADPt), 50 μL of the extracted samples were transferred to a 96-well plate. For detection of NADPH only, one tube of each sample was incubated at 60 °C for 30 min (to selectively degrade NADP$^+$), cooled on ice, and then 20 μL of the sample was transferred to the 96-well plate. Then, 100 μL of NADP Cycling Mix (98 μL of NADP Cycling Buffer Mix and 2 μL of NADP Cycling Enzyme Mix) was added to each well and the plate was incubated at RT for 5 min, followed by the addition of 10 μL of developer to each well and incubation for 2 h. Absorbance was read at 450 nm against an NADPH standard curve (0–100 pmol/well). The background value (control) was subtracted from all samples and the NADPH/NADP$^+$ ratio was calculated as: NADPH/(NADPt-NADPH).

Immunoblotting analysis

Forty-eight hours after treatment with FASNis, PDAC cells were harvested and lysed in 1 × cell lysis buffer (Cell Signaling Technology) containing protease and phosphatase inhibitors (Roche, Indianapolis, IN) for 30 min on ice with repeated mixing every 5 min. After protein concentrations were determined using the Pierce BCA® protein assay kit (Pierce, Rockford, IL), aliquots containing equal amounts of protein (50 μg) were resolved on 4–15 % polyacrylamide gels (Criterion TGX precast Gel; Bio-Rad, Hercules, CA) and transferred to PVDF membranes. Membranes were blocked with 5 % BSA or 10 % NFDM (nonfat dry milk) for 1 h at RT and incubated with primary antibodies overnight at 4 °C. Membranes were then washed three times with TBS-T, incubated with horseradish peroxidase-conjugated secondary antibodies (1:5,000) for 1 h at RT, visualized with Supersignal West Pico Plus Chemiluminescent Substrate (Pierce, Rockford, IL), and imaged with a LiCor Odyssey FC.

Quantitative reverse transcriptase-polymerase chain reaction

RNA was isolated using the Qiagen RNEasy plus mini kit according to the manufacturer's instructions. cDNA was synthesized using Superscript III First-Strand Synthesis (Life Technologies, Carlsbad, CA). Primer sets for qPCR were:

BIM (forward) ACCTGCAGATATGCGCCCAG
(reverse) ATTCGTGGGTGGTCTTCGGC
PUMA (forward) GGACGACCTCAACGCACAGT
(reverse) AATTGGGCTCCATCTCGGGG
NOXA (forward) GAGATGCCTGGGAAGAAG
(reverse) GCCGGAAGTTCAGTTTGT
BCL-2 (forward) ATCGCCCTGTGGATGACTGAGT
(reverse) GCCAGGAGAAATCAAACAGAGGC
BCL-X_L (forward) GCCACTTACCTGAATGACCACC
(reverse) AACCAGCGGTTGAAGCGTTCCT
MCL-1 (forward) CCAAGAAAGCTGCATCGAACCAT
(reverse) CAGCACATTCCTGATGCCACCT
HPRT (forward) GGCAGTATAATCCAAAGATGGTCAA
(reverse) GTCTGGCTTATATCCAACACTTCGT qPCR was performed on the ABI Prism 7900HT real-time system using a program consisting of 50 °C for 2 min, 95 °C for 10 min, then 40 cycles of 95 °C for 15 sec and 60 °C for 1 min. Data analysis was performed using the following equations: $\Delta C_t = C_t(\text{sample}) - C_t(\text{endogenous control})$; $\Delta\Delta C_t = \Delta C_t(\text{sample}) - \Delta C_t$ (untreated); and fold change $= 2^{-\Delta\Delta Ct}$.

Cell viability assay

The cell viability effects of the TVB FASNi TVB-3664 were determined using the colorimetric MTT (3-4,5-dimethylthiazol-2-yl-2,5-diphenyl-tetrazolium bromide) reduction assay. Dose-response curves were plotted as a percentage of the absorbance of control cells, which were obtained from vehicle-treated cells, to graded concentrations of TVB-3664. For each treatment, cell viability was evaluated using the following equation: (OD_{570} of the treated sample/OD_{570} of the untreated sample) × 100. Sensitivity to TVB-3664 was expressed in terms of the concentrations required for a 50 % (IC_{50}) reduction in cell viability. Since the percentage of control absorbance was considered to be the surviving fraction of cells, the IC_{50} values were defined as the concentration of drug that produced a 50 % reduction in control absorbance (by interpolation).

Xenograft studies

Xenografts were established by injecting 3.5×10^6 PANC-1, 5×10^6 MIA PaCa-2, 5×10^6 BxPC-3, 4×10^6 5160, 4×10^6 4041, and 4×10^6 6105 cells subcutaneously into the rear flank of *Foxn1^{nu}/Foxn1^{nu}* athymic mice (Harlan Sprague Dawley, Madison, WI). PANC-1, MIA PaCa-2, and BxPC3 xenografts were treated with TVB-3166 whereas the PDX models 4041, 5160, and 6105 were treated with TVB-3664. Once tumor engraftment was confirmed (>100 mm^3), mice (were randomly allocated to different treatment groups (n=10 per group).

i.) Vehicle (PEG-400)
ii.) TVB-3166 or TVB-3664 (2 mg/kg/day)
iii.) ABT-263 (100 mg/kg/day)
iv.) ABT-199 (100 mg/kg/day)
v.) TVB-3166/TVB-3664 (2 mg/kg/day) + ABT-263 (100 mg/kg/day)
vi.) TVB-3166/TVB-3664 (2 mg/kg/day) + ABT-199 (100 mg/kg/day).

All treatments were performed by oral gavage. Tumor volume was measured in 3D using a vernier caliper and calculated using the formula: tumor volume (mm^3) = (length x width x height)/2. Tumor volume values (mean ± S.E.) were calculated weekly for each experimental group over a 42-week period in a blinded fashion to minimize experimental bias. Antitumor activity was calculated for individual tumors as the percentage of tumor growth inhibition, using the formula: $100 - [(V_x/V_i) \times 100]$, where Vt is the tumor volume for treated mice and V_x is the tumor volume in the control group at a given x time point.

Statistical analysis

All cell-based observations were confirmed by at least three independent experiments performed in triplicate for each cell line and for each condition. Data are expressed as mean ± SD. Bar graphs, curves, and statistical analyses were generated using GraphPad Prism 10 (GraphPad Software, San Diego, CA). Two-group comparisons were

performed using Student's t-test for paired and unpaired values. Comparisons of means of ≥3 groups were performed by ANOVA, and the existence of individual differences, in the case of significant F values in ANOVA, was tested by Dunnett's multiple contrasts. p values < 0.05 and <0.005 were considered to be statistically significant (denoted as * and **, respectively). All statistical tests were two-tailed.

Results

The first-generation FASN inhibitor C75 sensitizes PANC-1 PDAC cells to the BCL2/BCL-X_L/BCL-W inhibitor ABT-263/navitoclax

To first assess whether FASN inhibition can be explored as an innovative means to overcome intrinsic mitochondrial apoptosis resistance in PDAC tumor cells, as we previously reported in breast cancer cells [52], the widely used *TP53* and *KRAS* mutant PANC-1 PDAC cell line was used as a proof-of-concept model. We investigated how pharmacological blockade of FASN activity with a preclinical FASN inhibitor, C75 –a synthetic analog of the antifungal antibiotic cerulenin that binds to the β-ketoacyl synthase (KS) and thioesterase (TE) domains of human FASN [53–56]– affects both the BCL-2 family interaction network, which controls the mitochondrial signaling pathway of cell death, and the response to the BCL2/BCL-X_L/BCL-W inhibitor ABT-263/navitoclax.

While treatment of PANC-1 cells with graded concentrations of C75 resulted in a robust, dose-dependent upregulation of the apoptogenic BH3-only BCL-2 members BIM, PUMA, and NOXA, no significant changes in the expression of the anti-apoptotic protein BCL-2 were observed (Fig. S1). FASN inhibition with C75 as a single agent promoted a slight increase in apoptotic cells as monitored by flow cytometry after double staining with propidium iodide (PI) and annexin V, which binds to the phosphatidylserine exposed by apoptotic cells (Fig. S1). The finding that FASN inhibition with C75 promoted a marked increase in proapoptotic BH3-only proteins, accompanied by an almost negligible cell death profile, strongly suggested an adaptive mechanism to tolerate FASN blockade. We hypothesized that pharmacological blockade of FASN activity could place PANC-1 PDAC cells in a primed-for-death state, "addicted" to anti-apoptotic proteins that sequester pro-apoptotic proteins to ensure survival, a phenomenon known as "mitochondrial priming" [27–29,57–59]. Given that FASN blockade results in the drastic upregulation of NOXA, a critical molecule that acts as an intrinsic and natural inhibitor of MCL-1 [60,61], we predicted that C75-treated PANC-1 cells should show an increased sensitivity to the BH3 mimetic drug such ABT-263/navitoclax, a potent and clinically pertinent antagonist of BCL-2, BCL-X_L and BCL-W [23–27]. While ABT-263/navitoclax alone failed to induce apoptotic cell death, C75-treated PANC-1 cells exhibited a significant enhancement of the pro-apoptotic effects of ABT-263/navitoclax (Fig. S1). When the cells were challenged with low serum medium to mimic a culture condition of exogenous lipid deprivation and reduce the uptake of free FAs, the combination of the FASNi C75 and ABT-263/navitoclax resulted in extremely high, synthetic lethal effects as evidenced by enhanced apoptotic cell death of PANC-1 cells (Fig. S1), confirming the FASN target specificity of C75 in sensitizing PDAC cells to ABT-263/navitoclax. These results suggest that the link between FASN-catalyzed *de novo* FA biosynthesis and the intrinsic mitochondrial apoptosis threshold is not limited to breast cancer cells [52], but rather appears to represent a pan-cancer function of FASN that can be exploited for therapeutic purposes in PDAC.

Computational deconvolution of next-generation TVB FASN inhibitors reveals uncompetitive mode of inhibition versus NADPH

First-generation FASNis such as C75 have failed to advance into the clinic due to unmanageable side effects [62,63]. 3-V Biosciences (now Sagimet Biosciences) has developed the so-called TVB series of orally bioavailable, reversible, potent, and selective next-generation FASNis. TVB-2640 (denifanstat) is the first FASNi in clinical trials [42,49,51,64,65]. Here, we took advantage of the denifanstat-related analogues TVB-3166 and TVB-3664 to explore the molecular relationship between FASN activity, oxidative stress/redox balance, and the intrinsic apoptotic pathway in PDAC cells. To highlight the molecular similarities and differences of TVB-2640, TVB-3166 and TVB-3664, we first performed a computational deconvolution of their mechanism of action.

The complete experimental crystal structure of human FASN has not yet been solved. However, the cryo-EM structure of the core modifying region of human FASN bound to the cofactor NADPH and TVB-2640/denifanstat was recently determined at 2.7 Å resolution [66]. Based on these crystallographic findings, it is proposed that TVB-2640 exerts its inhibitory effect by blocking the consumption of the NADPH cofactor by specifically binding to the KR domain of the FASN enzyme core modifying region [66] (Fig. S2A). Whether this mechanism of action extends to the TVB-2640 relatives, TVB-3166 and TVB-3664, remains to be investigated. Considering that quite similar experimental results can be obtained using isolated functional regions of human FASN rather than the complete structure of the enzyme [66,67], we built a model using the AlphaFold2 (AF2) neural network (see the "Materials and Methods" section for more details) containing only the ΨME:ΨKR:KR domains from the best-ranked AF2 structure (Fig. 1A; Fig. S2A). We generated a compact tri-domain structure of human FASN bound to the NADPH cofactor, which was used as a representative model to rationalize the binding mode in atomic detail and to predict the mechanism of action of TVB FASNis.

Although TVB-2640, TVB-3166, and TVB-3664 all share some structural similarities, there are some differences in their heterocycles that could have an electrostatic and steric effect in interacting with human FASN residues (Fig. 1A). Of note is the presence of a 1,2,4-triazole (TVB-2640), a pyrazole (TVB-3166) or an imidazole (TVB-3664) motif and their different substitution patterns (e.g., methyl, methoxy or trifluoromethyl groups). TVB-3664 imidazole and TVB-2640 triazole are predicted to exist in a tautomer that favors the formation of a hydrogen bond with Asp1977 (Fig. 1A, see Fig. S2B for additional tautomers considered). In contrast, the predicted binding pose of TVB-3166 shows that the nitrogen atoms of the pyrazole ring are exposed to the solvent and therefore do not interact with Asp1977 (Fig. 1A). Therefore, although all molecules can participate in hydrogen bonding through the nitrogen atoms, the pattern and strength is predicted to differ among TVB FASNis. In all cases, the TVB inhibitors are positioned at a hydrogen bonding distance from the catalytic Ser2021 and Tyr2034, as well as adjacent to the nicotine amide hydride donor of the NADPH cofactor, strongly supporting the notion that TVB molecules are uncompetitive FASNis toward the NADPH cofactor. Notably, this behavior is also consistent with the crystallographic binding mode previously reported for the KR-targeted FASNi GSK2194069 (Fig. S3) in complex with the FASN Psi/KR tri-domain, taking into the account the previously reported open conformation of the flexible loop (PDB code 4PIV; Fig. S3).

A clinical-grade FASNi promotes NADPH-dependent apoptotic cell death in PDAC cells

Given the putative mechanism of action described above, we decided to explore the therapeutic utility of clinical-grade TVB FASNis in disrupting the link between the NADPH-dependent FASN-catalyzed de novo FA biosynthesis and the intrinsic mitochondrial apoptotic threshold in established PDAC cancer cell lines such as PANC-1, MIA PaCa-2, and BxPC-3. The level of FASN expression in PANC-1 and MIA PaCa-2 cells is significantly higher than that in BxPC-3 cells [46].

We first sought to confirm whether treatment with TVB-3166 leads to NADPH accumulation in PDAC cells. Treatment with TVB-3166 resulted in a large, dose-dependent increase in the NADPH/$NADP^+$ ratio in "FASN-high" expressing PANC-1 and MiaPaCa-2 cells, but not in FASN-low BxPC-3 cells (Fig. 1B, *left panels*). Such a TVB-3166-induced increase in the NADPH/$NADP^+$ ratio was completely prevented in the

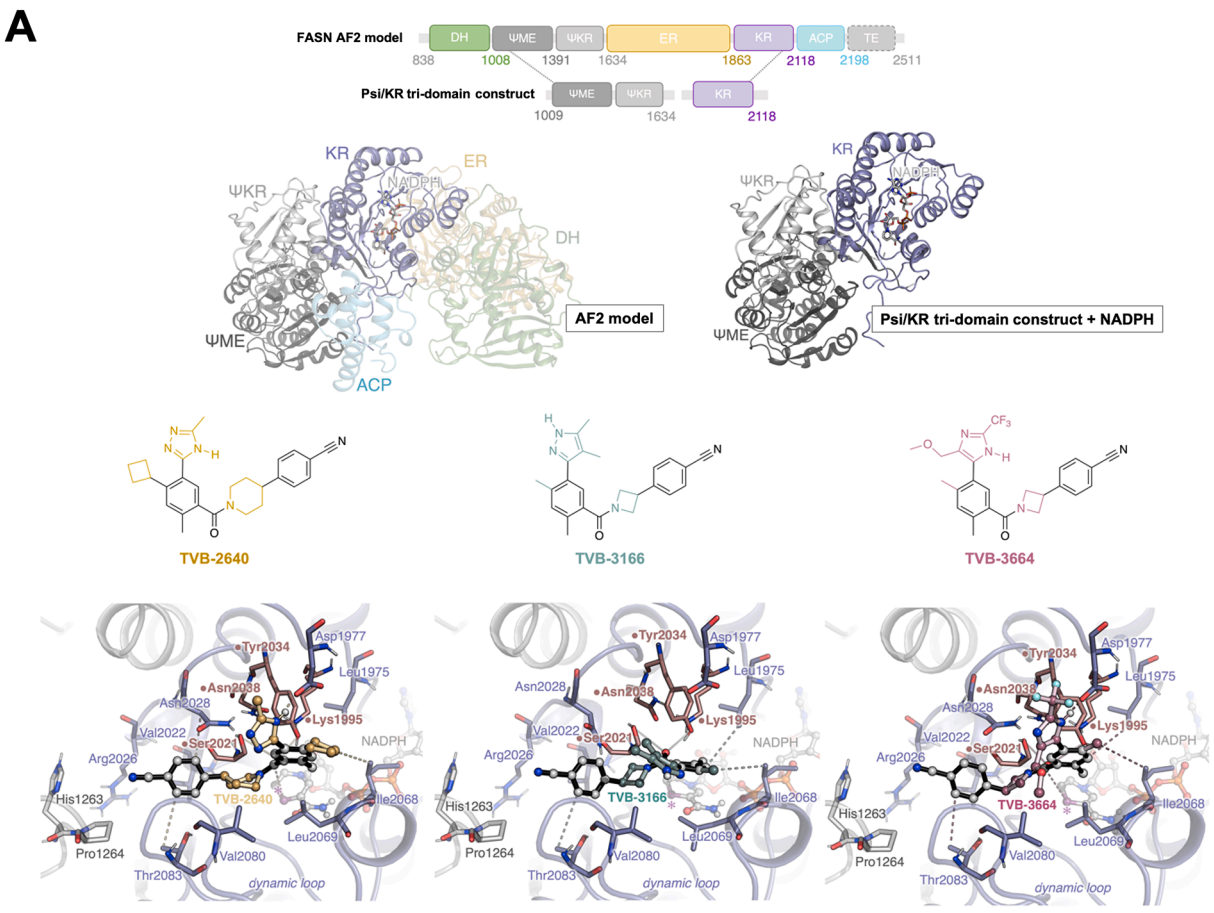

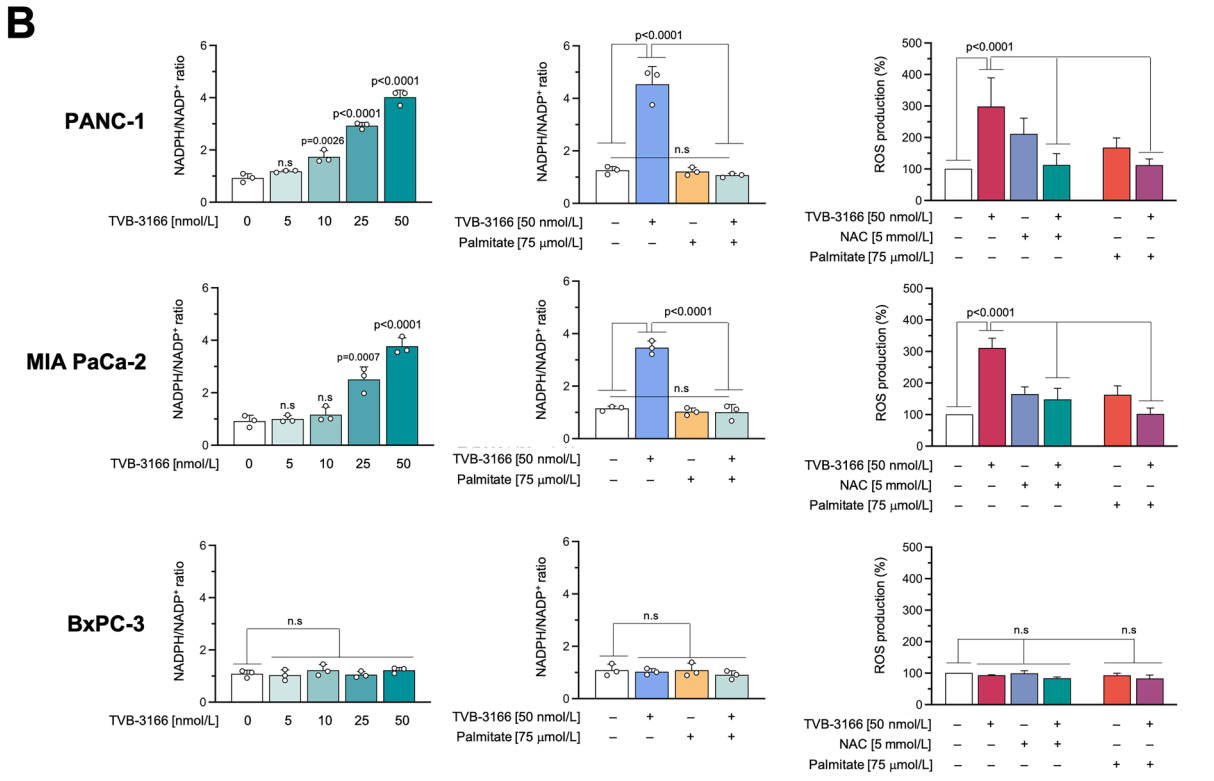

(caption on next page)

Fig. 1. TVB FASN inhibitors targeting the FASN ketoacyl reductase (KR) domain promote increased NADPH/NADP$^+$ ratios and ROS levels in PDAC cells. A. *Molecular interactions of TVB FASNis molecules with the FASN Psi/KR tri-domain. Top.* Linear and three-dimensional domain organization of the FASN core-modifying region AF2 model and Psi/KR tri-domain construct. Overlay of the three-dimensional representation of the AF2 structure of the human FASN core modifying region (up to the ACP domain) and the Psi/KR tridomain construct. The secondary structure is shown in cartoon mode and the NADPH cofactor at the KR catalytic core is shown in sticks. Psi/KR tridomain construct. Schematic representation of TVB-2640/denifanstat and its derivatives TVB-3166 and TVB-3664. Relevant functional regions that differ from each FASN inhibitor are highlighted in a different color: yellow for TVB-2640, teal for TVB-3166, and magenta for TVB-3664. *Bottom.* Detailed representation of the selected binding mode predicted by HADDOCK for each TVB molecule at the KR domain of the Psi/KR tridomain-NADPH structure. TVB-2640, TVB-3166, and TVB-3664 molecules are shown as sticks and spheres. Different regions are colored in yellow, teal, and magenta, respectively. Binding residues, in light blue, and catalytic residues (●), in brown, are shown as sticks only, while the nicotine amide hydride donor (✻), in gray, is also shown as spheres. For clarity, main chain atoms are omitted. Relevant non-covalent interactions are shown as dotted lines. Labels and numbering are specified according to the UniProtKB P49327 entry of the complete hFASN sequence or PDB code 8EYK. B. Fold-change of the NADPH/NADP$^+$ ratio and quantification of ROS in PANC-1, MIA PaCa-2, and BxPC3 PDAC cells treated with TVB-3166 in the absence or presence of palmitate or NAC for 48 h. Data are presented as mean ± SD (*n=3*). n.s., not significant.

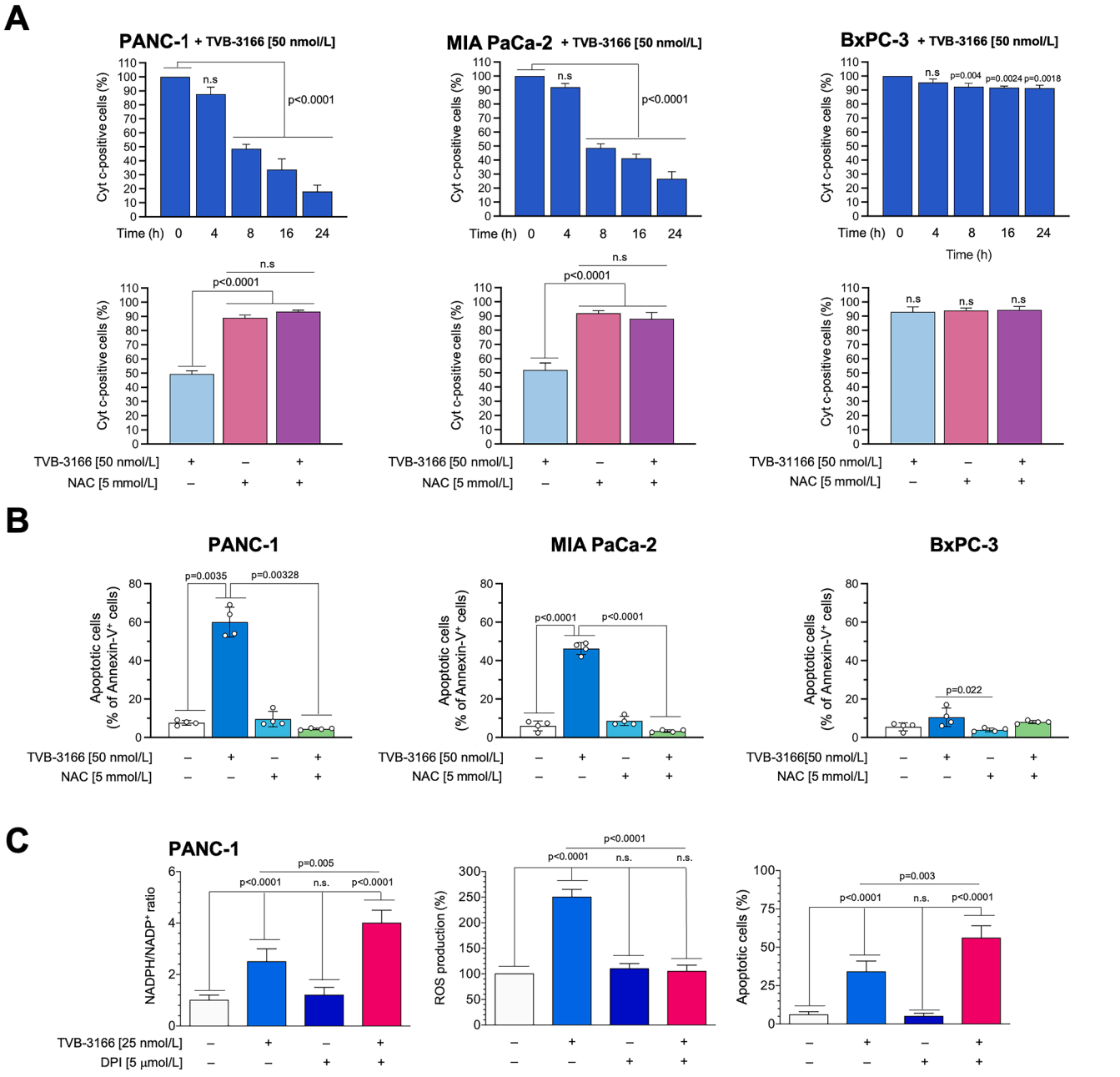

Fig. 2. The FASNi TVB-3166 promotes apoptotic cell death in established PDAC cells in a NOX/ROS-related manner. A. Flow cytometry-based assessment of mitochondrial cytochrome c after exposure to TVB-3166 (50 nmol/L) in the absence or presence of N-acetylcysteine (NAC, 5 mmol/L) for 48 h. Data are presented as mean ± SD (*n=3*). n.s., not significant. B. Annexin V/propidium iodide staining-based flow cytometric assessment of apoptotic cell death in PANC-1, MIA PaCa-2, and BxPC3 cells treated with TVB-3166 in the absence or presence of NAC. Data are presented as mean ± SD (*n=4*). n.s. not significant. C. Fold-change of the NADPH/NADP$^+$ ratio, quantification of ROS, and flow cytometric assessment of apoptotic cell death based on Annexin V/propidium iodide staining in PANC-1 cells treated with TVB-3166 in the absence or presence of the NOX inhibitor diphenyleneiodonium (DPI). Data are presented as mean ± SD (*n=3*). n.s., not significant.

presence of exogenously added palmitate (Fig. 1B, *middle panels*).

Next, we measured the production of reactive oxygen species (ROS) by the enhanced oxidation-dependent conversion of the non-fluorescent H_2DCFDA to the highly fluorescent 2′-7′-dichlorofluorescein (DCF). ROS production was significantly increased by TVB-3166 in PANC-1 and MIA PaCa-2 cells, but not in BxPC-3 cells (Fig. 1B, *right panels)*. The ability of TVB-3166 to promote ROS accumulation in TVB-3166-sensitive PANC-1 and MIA PaCa-2 cells was blocked either by co-treatment with the ROS scavenger N-acetylcysteine (NAC) or by addition of the FASN end product palmitate (Fig. 1B, *right panels*).

Rescue experiments with NAC and palmitate appear to accurately link the blockade of NADPH consumption imposed by the predicted mechanism of action of TVB-3166 with an increased production of intracellular ROS. Because the release of cytochrome c (cyt c) from the mitochondrial intermembrane space into the cytosol is a key step in the early stages of mitochondrial apoptosis that ultimately triggers the caspase cascade [67,68], we sought to determine whether ROS production might be a key driver of the apoptotic response to TVB-3166 by measuring time-dependent cyt c release by flow cytometry in the absence or presence of NAC. Treatment with TVB-3166 significantly reduced the number of cyt c-positive cells in a dose-dependent manner in FASN-high expressing PANC-1 and MIA PaCa-2 cells, but not in FASN-low expressing BxPC-3 cells (Fig. 2A, *top panels*). Co-treatment with the ROS scavenger NAC, completely blocked the ability of FASNi TVB-3166 to promote cyt c release in PANC-1 and MIA PaCa-2 cells (Fig. 2A, *bottom panels*). We then monitored TVB-3166-induced apoptosis using Annexin V for the flow cytometric detection of externalized phosphatidylserine at intermediate stages of apoptosis. Exposure to TVB-3166 strongly increased the number of Annexin V-positive apoptotic cells in FASN-high expressing PANC-1 and MiaPaCa-2 PDAC cell lines by ~ 8 to 9-fold compared to FASN-low expressing BxPC-3 cells, which were insensitive to the pro-apoptotic effects of TVB-3166 (Fig. 2B). Co-treatment with NAC significantly reduced the appearance of annexin V-positive cells in response to TVB-3166 (Fig. 2B), thereby suggesting that ROS-generating mechanisms may play an important role in the apoptotic activity of TVB FASNis.

To determine whether FASN activity is linked to PDAC cytoprotection via the control of the NADPH/$NADP^+$ balance and/or ROS production, we replaced NAC, a synthetic precursor of intracellular cysteine and glutathione (GSH) [69,70], with diphenyleneiodonium (DPI), a potent inhibitor of the cellular redox metabolism that induces oxidative stress by blocking NADPH oxidase activity [71,72]. While NAC prevented TVB-3166-induced increases in the NADPH/$NADP^+$ ratio, intracellular ROS, and apoptotic cell death, DPI mimicked NAC to similarly prevent TVB-3166-induced ROS but further potentiated TVB-3166-induced NADPH accumulation and apoptotic cell death (Fig. 2C). These findings suggest that high levels of ROS are induced but not responsible for TVB-3166-induced apoptotic cell death in PDAC cancer cells; rather, PDAC-associated FASN activity appears to play a central role in maintaining cellular redox homeostasis and its inhibition leads to NADPH accumulation-mediated apoptosis (73,74; Fig. 3A).

A clinical-grade FASNi sensitizes FASN-positive PDAC cells to BH3 mimetics

Mitochondrial priming of the apoptotic machinery has been shown to sensitize cultured PDAC tumor cells to the cytotoxic effects of conventional chemotherapy [17–20,75–77]. To test the premise that manipulation of mitochondrial priming with a targeted FASNi enhances the efficacy of BH3 mimetics, we investigated whether the FASNi TVB-3166 sensitizes FASN-positive PDAC cells to the BH3 mimetics ABT-263/navitoclax and ABT-199/venetoclax. In the presence of a suboptimal concentration of TVB-3166 (10 nmol/L), we observed a dramatic enhancement of the ability of BH3 mimetics to promote apoptotic cell death in FASN-high expressing PANC-1 and MiaPaCa-2 PDAC cell lines, but not in FASN-low expressing BxPC-3 cells, which remained largely insensitive to the synergistic pro-apoptotic effects of TVB-3166 plus BH3 mimetics (Fig. 3B). In contrast, the single agents ABT-263/navitoclax and ABT-199/venetoclax were largely inefficient in inducing significant levels of apoptotic cell death in PDAC cell lines (Fig. 3B). PANC-1 and MiaPaCa-2 cells were exquisitely sensitive to the sensitizing effects of TVB-3166, which increased the apoptotic activity of ABT-263/navitoclax and ABT-199/venetoclax by more than 7 to 8-fold, reaching Annexin V-positive apoptotic cell proportions as high as 70 % (Fig. 3B). An optimal concentration of TVB-3166 (50 nmol/L) induced high levels of apoptotic cell death as a single agent in FASN-overexpressing PDAC cell lines. Such an optimal concentration of TVB-3166 caused a lower degree of potentiation of the pro-apoptotic activity of BH3 mimetics (Fig. S5), clearly indicating a threshold sensitizing effect of FASN blockade on mitochondrial priming.

We then evaluated the ability of the FASNi TVB-3166 to sensitize PDAC xenografted tumors to BH3 mimetics *in vivo* (Fig. 3C). Both TVB-3166 and the BH3 mimetics were administered by oral gavage to mimic the oral drug administration in humans. Both ABT-263/navitoclax and ABT-199/venetoclax failed to reduce PANC-1 and BxPC3 xenograft tumor growth when administered as single agents. The single agent FASNi TVB-3166 was moderately effective in inducing a tumor response in PANC-1 tumors with high FASN expression (33 % tumor growth inhibition; Fig. 3C) and completely ineffective in BxPC3 tumors with low FASN expression (Fig. S6). The complete lack of anti-tumor efficacy of ABT-263/navitoclax and ABT-199/venetoclax as single agents was significantly overcome when PANC-1 tumor xenografts were co-treated with TVB-3166, a combination that achieved tumor growth inhibition rates as high as 65–70 % (Fig. 3C). In BxPC3 tumors, no interaction was observed between FASNi TVB-3664 and BH3 mimetics (Fig. S6). The sensitizing effects of FASNis to navitoclax/ABT-263 and venetoclax/ABT-199, both *in vitro* and in *in vivo* xenografted tumors, strongly suggest that FASN blockade synergizes with BH3 mimetics by lowering the apoptotic threshold of PDAC cells.

A clinical-grade FASNi modifies the BCL-2 interactome in cell lines developed from patient-derived xenografts (PDXs)

In contrast to traditional PDAC cell lines (e.g., PANC-1), recently developed patient-derived xenograft (PDX) cell lines more closely mimic the molecular and transcriptional characteristics of PDAC tumors [78–81], including the corresponding PDAC molecular subtypes [82,83]. PDX-derived tumor cells can be used to better predict and empirically determine of the clinical relevance of novel therapeutic approaches against PDAC such as FASNis. First, we obtained 10 unique PDX-derived cell lines [81,84,85] and characterized the expression status of the FASN protein (Fig. 4A, *left panels*). The highest levels of FASN protein were found in models 6105, 4535, and 6164, three PDX-derived cell lines of the *classical* (*pancreatic*) PDAC transcriptomic subtype with a low replication stress signature [81–83]. Intermediate levels of FASN were observed in models 5641 and 4041, the latter representing a unique model of the *classical* (*pancreatic*) transcriptomic PDAC subtype with a high replication stress signature [81–83] (Fig. 4A, *left panels*). Low levels of FASN were found in five PDX-derived cell lines, namely 4666, 5160, 6052, 4911, and 4833, the latter two PDX-derived models belonging to the *squamous* transcriptomic PDAC subtype [81–83].

The following *in vivo* studies were performed with TVB-3664, a TVB-3166-related molecule that has been shown to have higher potency against human FASN while maintaining an excellent bioavailability and pharmacokinetic properties in mice [65]. Among the 10 PDX-derived PDAC cell lines, 5160, 4041, and 6105 were selected as models of low, intermediate, and high FASN expression status. MTT-based cytotoxicity assays revealed that TVB-3664 produced a dose-dependent reduction in the number of viable PDX-derived tumor cells that notably varied among cell lines. When differences between cell line sensitivities were evaluated by calculating the half-maximal inhibitory concentrations (IC_{50}), TVB-3664 IC_{50} values ranged from less than 1

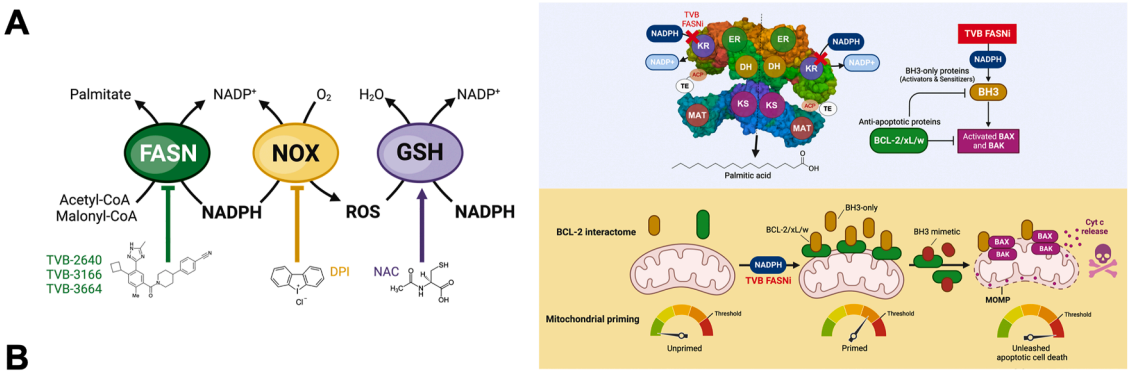

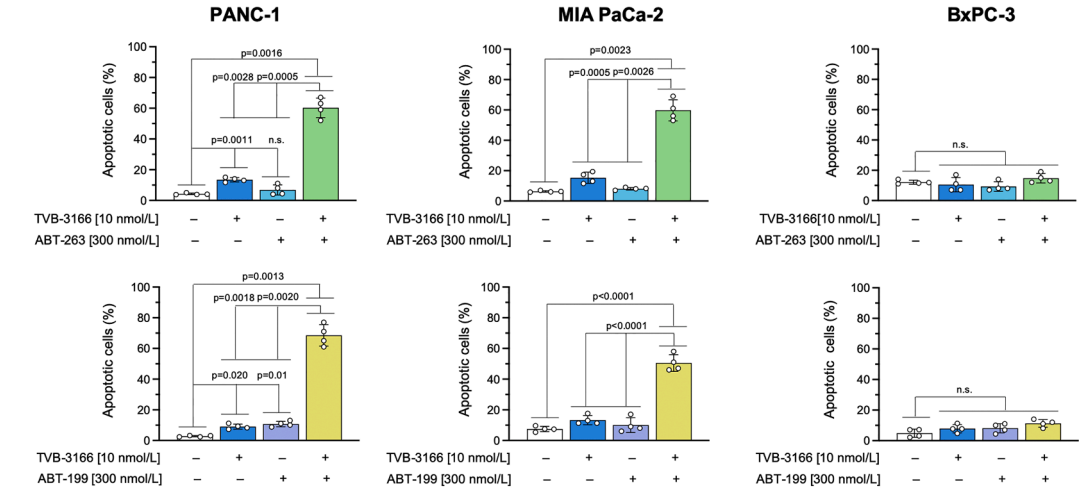

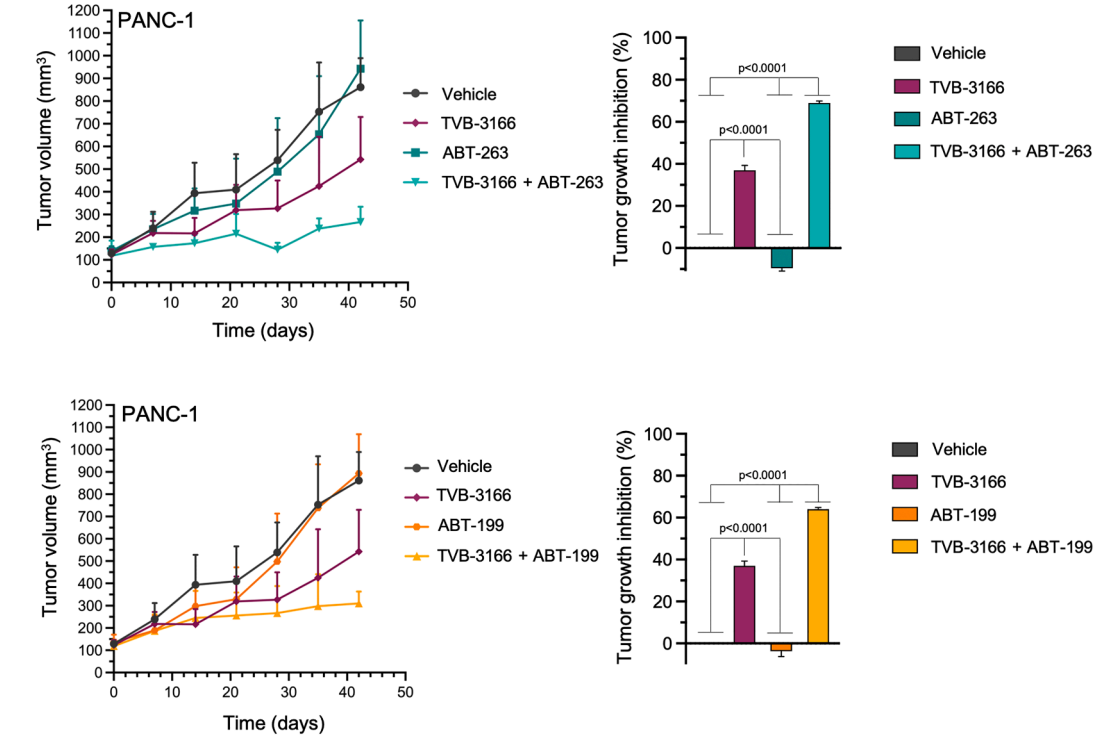

(caption on next page)

Fig. 3. FASN inhibition sensitizes established PDAC cells to the pro-apoptotic effects of BCL2 inhibitors *in vitro* and *in vivo*. A. *Left.* FASN inhibition leads to the accumulation of its substrate NADPH. The accumulated NADPH activates NOX to generate ROS as a means to restore redox homeostasis of the altered NADPH/$NADP^+$ ratio via the glutathione system. The NOX inhibitor DPI blocks NOX-mediated ROS generation but potentiates further FASNi-induced NADPH accumulation. The glutathione precursor NAC scavenges ROS by boosting the glutathione system, thereby reducing both ROS levels and the NADPH/$NADP^+$ ratio. DPI promotes while NAC prevents FASNi-induced apoptotic cell death in PDAC cells. *Right.* FASN inhibition links NADPH to mitochondrial apoptotic priming. In FASN-positive PDAC cells, mitochondria have a low BH3-only protein load leaving excess pro-survival BCL-2 proteins to neutralize BH3-only proteins resulting from treatment with pro-apoptotic BH3-mimetics (unprimed state). The metabolic stress caused by FASN blockade (i.e., NADPH/ROS accumulation) results in a high BH3 only protein load that is largely counteracted by pro-survival BCL-2 members. Thus, FASNis shift the balance between pro- and anti-apoptotic proteins closer to the apoptotic threshold, a reorganization of the BCL2 interactome that reduces the stochiometric amount of BH3 proteins required to cross the threshold for MOMP and death of PDAC cells (primed state). Co-treatment with BH3 mimetics, small synthetic molecules that bind one or more anti-apoptotic BCL-2 regulators and displace the endogenous BH3-only proteins, results in excess activator BH3-only proteins that cause BAX/BAK activation and act synergistically to push PDAC cells beyond the apoptotic threshold, thereby triggering apoptotic cell death. B. Annexin V/propidium iodide staining-based flow cytometric assessment of apoptotic cell death in PANC-1, MIA PaCa-2, and BxPC3 cells treated with a sub-optimal dose of TVB-3166 (10 nmol/L) in the absence or presence of ABT-263/navitoclax or ABT-199/venetoclax. Data are presented as mean ± SD (*n=4*). n.s., not significant. C. Subqutaneous growth of PANC-1 xenografts in athymic mice treated with the BH3 mimetics navitoclax/ABT-263 (*top*) and venetoclax/ABT-199 (*bottom*) in the absence or presence of the FASNi TVB-3166. The maximum duration of each treatment was 42 days. Results are presented as the mean tumor volume ± S.D. (*n*=10 mice/experimental group). Tumor growth inhibition (TGI) was calculated as the percentage of tumor growth, relative to tumor size at baseline in the drug-treated groups compared to the vehicle-treated (control) group.

nmol/L in 6105 cells to approximately 45 nmol/L in 5160 cells (>50-fold difference; Fig. 4A, *right panels*). In the case of TVB-3166, an IC_{50} value of approximately 50 nmol/L could be solely calculated in 6105 cells whereas IC_{50} values were not reached within the concentration range tested in 4041 and 5160 cells (data not shown). By scoring the sensitivity of the cells to TVB FASNis, we can rank the cell lines from the most resistant to the most sensitive as follows: 5160 >> 4041 > 6105 (Fig. 4A, *right panels*). These findings clearly highlighted the close correlation between FASN expression status and the sensitive (6105 and 4041) versus resistant (5160) phenotype of PDX-derived PDAC cells. Treatment with TVB-3664 resulted in a dose-dependent increase in the NADPH/$NADP^+$ ratio in patient-derived PDAC cell lines, particularly in the 4041 and 6104 models (Fig. 4B, *top panels*). The TVB-3646-induced increase in the NADPH/$NADP^+$ ratio was completely prevented in the presence of exogenously added palmitate (Fig. 4B, *bottom panels*).

To explore the molecular mechanisms underlying the cytotoxic effects of TVB-3664 against the PDX-derived cell lines, we examined the effect of FASN blockade on the death decision circuit controlled by the BCL-2 protein family (Fig. 4C). Expression of the anti-apoptotic/pro-survival proteins BCL-2 and BCL-X_L remained largely unaltered in response to graded concentrations of TVB-3664 (48 h) in all the PDX models, regardless of their intrinsic sensitivity to the FASNi (Fig. 4C, *left panels*); expression of the anti-apoptotic MCL-1 protein was significantly up-regulated in response to TVB-3364 in (TVB-3364-resistant) 5160 cells, slightly activated in 4041 cells, and remained unchanged in (TVB-3364-sensitive) 6105 cells. TVB-3364 promoted a marked, dose-dependent activation of the pro-death BH3-only protein BIM, which promiscuously binds to all the anti-apoptotic BCL-2 family members and is a probe of general mitochondrial priming. TVB-3364 promoted the hyperactivation of the three alternatively spliced BIM isoforms (BIM_{EL}, BIM_L, BIM_S), which are known to have different pro-apoptotic potentials, with the smaller species BIM_S and BIM_L being the most potent killers and BIM_{EL} the weakest. While TVB-3364-induced BIM accumulation was somewhat more pronounced in TVB-3364-responsive 6105 cells, the strong up-regulation of BIM occurred independently of the intrinsic sensitivity of the PDX cancer cells to TVB-3364. Similarly, the TVB-3364-induced dose-dependent accumulation of the pro-death BH3-only proteins PUMA and NOXA was more pronounced in TVB-3364-responsive 6105 cells, but occurred in all the PDX cancer cell models regardless of their intrinsic sensitivity to the FASNi (Fig. 4C, *left panels*).

Since the expression of the pro-apoptotic "BH3 domain only" BIM, PUMA, and NOXA is transcriptionally regulated during apoptosis [86–89], we examined whether the observed TVB-3364-induced changes in the BCL-2 interactome at the protein level were triggered by previous transcriptional changes in anti- and pro-apoptotic gene expression (Fig. 4C, *right panels*). qRT-PCR analyses of *BIM, PUMA*, and *NOXA* mRNAs revealed that NOXA showed the strongest induction after 24 h of treatment with graded concentrations of TVB-3364, followed by PUMA and BIM, which showed mild to strong upregulation responses. No significant changes in the levels of pro-survival BCL-2, BCL-X_L or MCL-1 mRNAs were detected in any of the PDX models even at the highest concentration of TVB-3664. Taken together, these data suggest that transcriptional upregulation of BIM, PUMA, and NOXA is a core pro-apoptotic mode activated by FASN blockade in PDX PDAC cells.

A clinical-grade FASNi sensitizes PDX-derived PDAC cell lines to BH3 mimetics

To support the clinical relevance that PDX-derived cell lines acquire an apoptosis-prone state upon FASN inhibition that may be highly sensitive to BH3 mimetics, we performed *in vitro* and *in vivo* studies to explore the nature of the interaction between a targeted FASNi and BH3 mimetics in these models. While ABT-263/navitoclax and ABT-199/venetoclax failed to induce apoptotic cell death as single agents, the combination of TVB-3664 and BH3 mimetics resulted in extremely high, synthetic lethal apoptotic effects (up to 7- to 8-fold increase) in 4041 and 6105 PDX-derived models (Fig. 5). Using an optimal concentration of TVB-3664 (50 nmol/L), which induces high levels of apoptotic cell death as a single agent, we observed a lesser degree of potentiation of the pro-apoptotic activity of BH3 mimetics that was restricted to TVB-3644-responsive 4041 and 6105 PDAC cells (Fig. S7), once again suggesting a threshold sensitizing effect of FASN blockade on apoptotic priming.

Single agent ABT-263/navitoclax and ABT-199/venetoclax slightly reduced tumor growth (up to 20 % reduction) only in the model 6105 but not in 4041 (Fig. 5). A suboptimal dose of single agent TVB-3664 was moderately effective in inducing an inhibitory tumor response against 6105 and 4041 models (26 % and 35 % reduction, respectively). Co-treatment of the 6105 with TVB-3664 and either ABT-263/navitoclax or ABT-199/venetoclax resulted in tumor growth inhibition (TGI) rates as high as 65 % (in the combination of TVB-3664 plus venetoclax/ABT-199). This synergistic interaction was even more evident in the 4041 model, whose tumors were completely refractory to ABT-263/navitoclax and ABT-199/venetoclax monotherapy, but achieved highly significant tumor responses –up to 71 % TGI rates– when combined with TVB-3664 (Fig. 5). Thus, FASN blockade with a clinical-grade FASNi therefore synergizes with BCL2 inhibitors to reduce tumor growth of patient-derived PDAC cells *in vivo*.

Discussion

Therapeutics with novel mechanisms of action are urgently needed to improve the dismal prognosis of PDAC. Here, we show that the oncometabolic enzyme FASN links the activation status of endogenous FA biosynthesis to the intrinsic apoptotic threshold in PDAC cells, which can be exploited therapeutically by combining clinical-grade TVB FASNis with BH3 mimetics to overcome mitochondrial apoptosis resistance

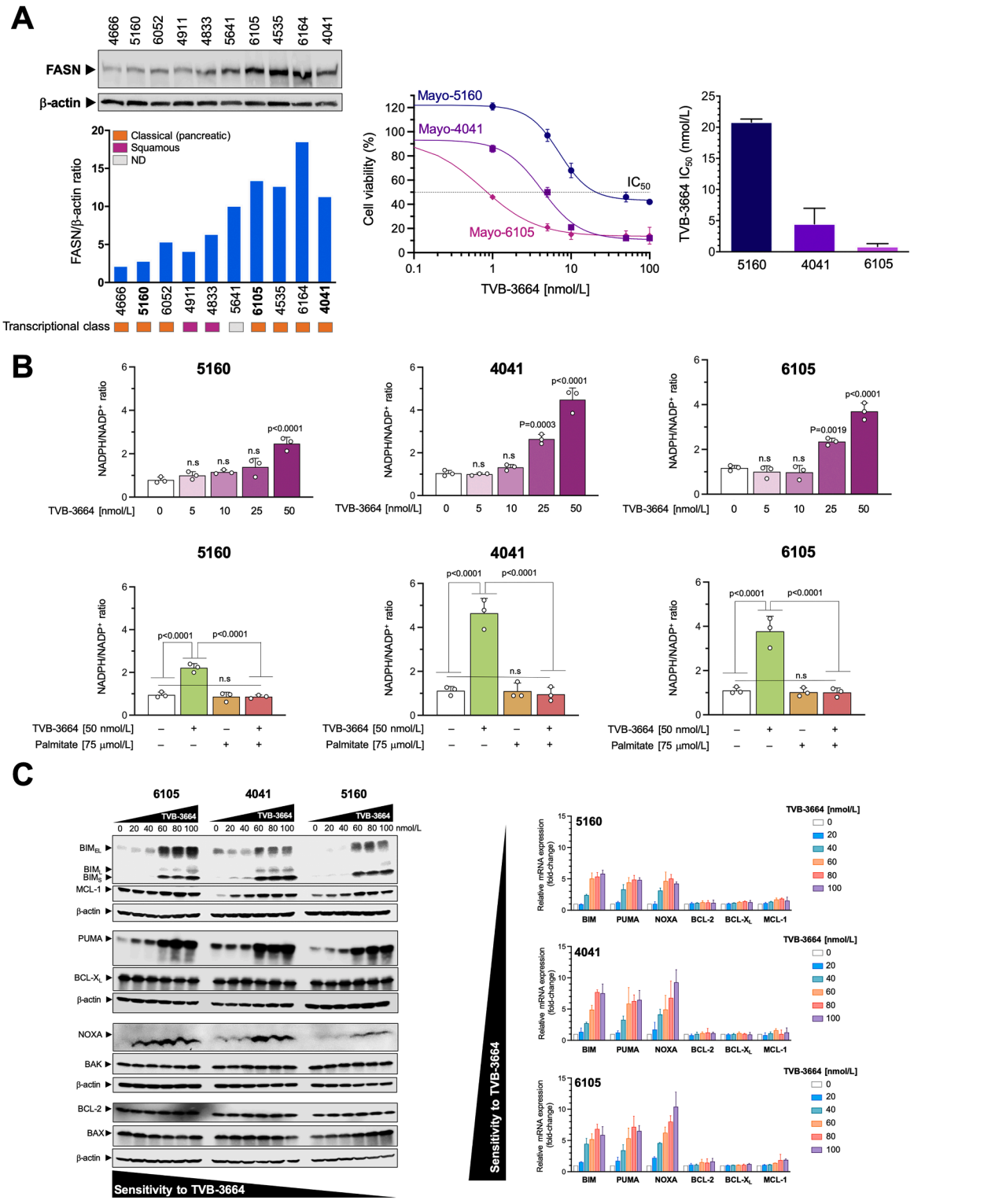

Fig. 4. TVB-FASNis reduce cell viability and activates the expression of pro-apoptotic BH3 only-proteins in patient-derived PDAC cells. A. Evaluation of the relationship between FASN expression status and sensitivity of patient-derived PDAC cells to the TVB FASNi TVB-3664. *Left.* Representative immunoblot analysis of FASN protein expression and relative expression of FASN normalized to β-actin in a panel of patient-derived PDAC cells. ND, not determined. *Right.* Dose-response cell viability curves of patient-derived 5160, 4041, and 6105 PDAC cells treated with graded concentrations of TVB-3664. Half-maximal inhibitory concentration (IC_{50}) values of TVB-3664 in patient-derived 5160, 4041, and 6105 PDAC cells are presented as mean (*columns*) ± SD (*bars*) (n=3). B. Fold-change of the $NADPH/NADP^+$ ratio in patient-derived 5160, 4041, and 6105 PDAC cells treated with TVB-3664 in the absence or presence of palmitate. Data are presented as mean ± SD (n=*3*). n. s., not significant. C. Evaluation of the relationship between TVB-3664 sensitivity and alteration of the BCL2 interactome. *Left.* Representative immunoblotting analysis of BIM, MCL-1, PUMA, $BCL\text{-}X_L$, NOXA, BAK, BCL-2, and BAX in TVB-3664 in patient-derived 5160, 4041, and 6105 PDAC cells treated with graded concentrations of TVB-3664 for 48 h. *Right.* qRT-PCR analyses of the expression of *BIM, PUMA, NOXA, BCL-2, BCL-X$_L$*, and *MCL-1* genes in patient-derived 5160, 4041, and 6105 PDAC cells treated with graded concentrations of TVB-3664 for 48 h. Data are presented as mean ± SD (n=*3*).

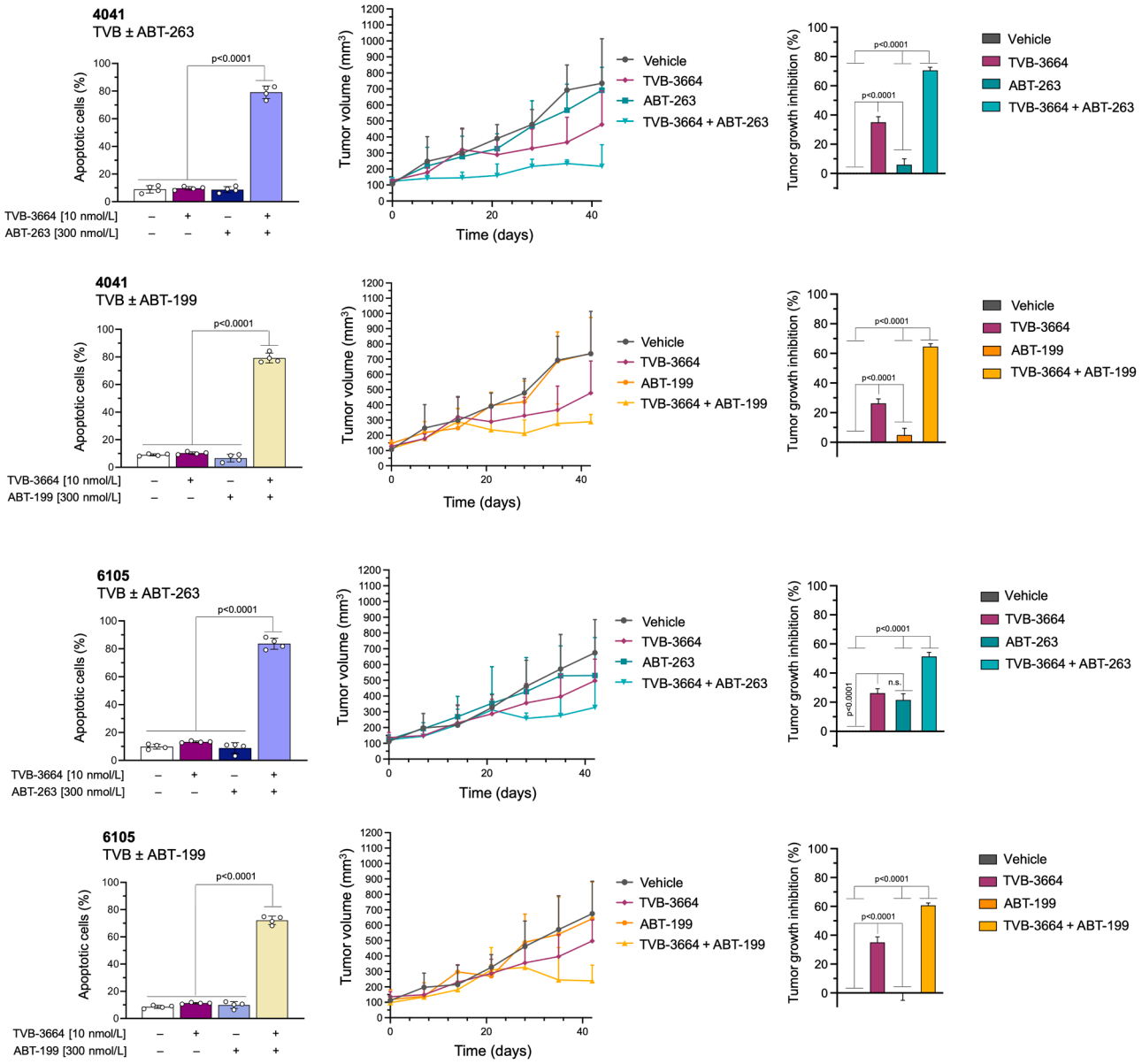

Fig. 5. FASN inhibition sensitizes patient-derived PDAC cells to the pro-apoptotic effects of BCL2 inhibitors *in vivo*. Subqutaneous growth of 4041 and 6105 PDX-derived cell lines in athymic mice treated with the BH3 mimetics navitoclax/ABT-263 and venetoclax/ABT-199 in the absence or presence of the FASNi TVB-3664. The maximum duration of each treatment was 42 days. Results are presented as the mean tumor volume ± S.D. (n=10 mice/experimental group). Tumor growth inhibition (TGI) was calculated as the percentage of tumor growth, relative to tumor size at baseline in drug-treated groups compared to vehicle-treated (control) group.

in PDAC.

Most cancer cells, including PDAC cells, are often dependent on FASN-driven *de novo* FA biogenesis and are therefore more sensitive than normal cells to pharmacological disruption of the lipogenic pathway. Despite strong support for FASN as an oncology target for therapeutic intervention, most FASNis have not been explored in the clinic due to low cellular permeability, irreversible binding, unwanted reactivity, lack of specificity, and/or unmanageable side effects (such as increased whole-body energy expenditure and significant body weight loss), the latter including the widely used tool compounds cerulenin and C75 [reviewed in 42]. Although remarkable structural and medicinal chemistry efforts have generated a large repertoire of small molecule inhibitors of the seven distinct catalytic domains of FASN, no compounds other than TVB-2640 have reached the clinic. Denifanstat (TVB-2640), an imidazopyridine-based reversible inhibitor of the KR domain of FASN, is the only orally bioactive, once-daily dosed FASNi with improved pharmacokinetic properties currently in clinical trials [42, 49–51].

We revisited the atomic modeling of the core modifying region of human FASN in complex with either TVB FASNis (TVB-3166, TVB-3664, and TVB-2640/denifanstat) or the small triazolone GSK2194069, another specific inhibitor of the KR activity of FASN. Despite their structural modifications, the nitrile moiety of all three TVB molecules was positioned in the same region of the hydrophobic side of the ΨME:Ψ KR:KR tri-domain. In addition to polar contacts, TVB molecules were also found to form hydrophobic contacts with residues of the KR-ΨME cavity, such as Leu1975, Val2022, Ile2068, Leu2069, Val2080, and Thr2083. The position of the most variable groups between the three TVB molecules (*i.e.*, methyl/cyclobutyl and the heterocycle rings) were all oriented toward a previously defined flexible loop that interacts with the acyl carrier protein (ACP) region (Fig. S4) [66,67]. Thus, our computational studies not only support that TVB FASNis block FASN

consumption of NADPH via an uncompetitive behavior towards NADPH when bound to the KR domain of FASN, but also suggest that further refinements should be made to understand the mechanistic importance of FASNis located in the ACP binding regions, indeed adjacent to the Ser2156 residue that will ultimately hold the acyl chain during FA biosynthesis.

The level of NADPH accumulation appears to mechanistically underlie the sensitivity of PDAC cells to the induction of apoptotic cell death by TVB FASNis. NADPH levels increased much more in cell lines with high or intermediate FASNi sensitivity than in models with low FASNi sensitivity. Although it is well known that NADPH consumption by FASN lipogenic activity is a key component of cellular redox homeostasis [90], the exact mechanism by which elevated NADPH levels lead to an increased apoptotic priming and increased dependence on antiapoptotic BCL2 members remains to be fully elucidated. Current evidence indicates that TVB FASNis-driven NADPH accumulation fuels ROS production via its role as a substrate for the NADPH oxidases (NOXs) [75,91–93]. Consistent with this view, only when ROS suppression is accompanied by prevention of NADPH accumulation can the apoptotic priming activity of FASNis be prevented, whereas the apoptotic efficacy of FASNis is maximized when the excess of NADPH cannot be scavenged by the activity of NOXs. Because accumulation of intracellular NADPH can lead to levels of ROS production that overwhelm ROS scavenging capabilities, it would be interesting to test whether the ability of FASNis to disrupt the delicate balance between NADPH-dependent protection against oxidative stress and the so-called NADPH-dependent "reductive stress" [94–97] –an abnormally high reducing molecular environment generated in response to uncontrolled elevation of the NADPH/$NADP^+$ ratio– is the molecular conduit linking FASN activity to the BCL-2 interactome. Because reorganization of the BCL-2 interactome allows cells to regulate the switch between adaptive and pro-apoptotic phases in response to elevated states of oxidative injury, further investigation is needed to definitively establish how perturbation of FASN-regulated NADPH pools increases the mitochondrial apoptotic priming in terms of transcriptional activation of pro-apoptotic proteins (e.g., BIM, PUMA, NOXA). Moreover, if NADPH accumulation is the ultimate metabolic trigger that primes PDAC cells for mitochondrial apoptosis in response to TVB FASNis, next-generation "NAXibs" (NADPH oxidase inhibitors) [93,98,99] could be explored as combination boosters to unlock the full therapeutic potential of TVB FASNis as mitochondrial apoptotic drugs.

As with other metabolism perturbing small molecules [100], another reason why previous efforts to alter FASN-driven endogenous lipogenesis by chemical inhibition may have failed is that they have relied solely on measuring cancer cell survival using a binary cell fate (life vs death). We have recently taken an alternative approach based on the notion that FASN-targeting drugs could regulate how "primed for death" cancer cells are, which depend on the dynamic interplay between pro- and anti-apoptotic members of the BCL-2 protein family as key regulators of MOMP, the critical event that commits a cell to apoptosis [42]. As previously reported in breast cancer cells [52], TVB FASNis promote the increased transcription and synthesis of several pro-death, BH3-only activator proteins including BIM, PUMA and NOXA –the sentinels of cellular stress whose activation commits cells to apoptosis– in lipogenic PDAC cells. However, the elevated levels of anti-apoptotic BCL-2 proteins lead to sequestration of the pro-apoptotic proteins and prevent cell death in a significant number of PDAC cells. Thus, pharmacological disruption of FASN activity promotes a threshold crossing phenomenon of fractional killing in which some PDAC cancer cells are killed, but the majority switch to a higher state of death *readiness* that is dependent on certain anti-apoptotic proteins to sequester BH3-only proteins and ensure survival [42]. Treatment of PDAC cells with TVB FASNis thus sensitizes them to subsequent treatment with BH3 mimetics, a class of small molecules that facilitate the action of proapoptotic proteins by binding to the antiapoptotic proteins, causing them to release BIM, PUMA, and NOXA, which can in turn can act as direct activators of BAX and/or BAK. From a therapeutic perspective, the resistance of PDAC to mitochondrial apoptosis when using targeted therapies such as BH3 mimetics is largely due to their constitutive high levels of MCL-1. BH3 mimetics that interact with BCL-X_L and/or BCL-2 are expected to result in the release of sequestered BIM and PUMA that which are captured by MCL-1 before they can activate BAX or BAK. Therefore, a proposed strategy to sensitize PDAC cells to BCL-2/BCL-X_L/BCL-W and BCL-2-specific BH3 mimetics involves the activation of NOXA, a BH3-only protein that is relatively selective in blocking MCL-1 (as it can also interact with BCL-X_L and BCL-2, albeit with lower affinities) [101]. If NOXA expression can be enforced, high levels of NOXA will efficiently sequester MCL-1 to allow the release and subsequent activation of BAK/BAX upon binding of BCL-X_L and/or BCL2 by ABT-263/ABT-199 BH3 mimetics [17,102–104]. Our results strongly suggest that TVB FASNis could serve as *bona fide* NOXA inducers and, in combination with BCL2 inhibitors, could be used to directly activate the cell death machinery to overcome resistance of PDAC to mitochondrial apoptosis (Fig. 6).

In the context of solid tumors, including PDAC, beyond some *in vitro* reports of the dependence of established PDAC cells on the anti-apoptotic homologues BCL-2, BCL-X_L, and MCL-1 and the enhancement of gemcitabine sensitivity by the BCL2i ABT-199/venetoclax [19,101–104], little is known about the efficacy of BH3 mimetics as single agents or in combination regimens, and to date no clinical trials of BH3 mimetics are ongoing in PDAC (www.clinicaltrials.gov). The fact that FASN-inhibited PDAC cells exist in an apoptosis-prone state that is highly sensitive to BH3 mimetics identifies a mitochondrial sensitization phenomenon that may improve their therapeutic index in PDAC patients. One of the strengths of our study is that we provide evidence for the combinatorial antitumor efficacy of clinical-grade TVB FASNis and BH3 mimetics in preclinical models of PDAC patient-derived cancer cell lines, mostly representative of the classical pancreatic lineage of the recently described transcriptomic subtypes of PDAC. Higher levels of FASN appear to occur in DNA damage response (DDR) proficient PDAC cells and, in particular, in those that additionally exhibit a low replication stress transcriptional signature. Although DDR proficient/low replication stress PDAC cells do not benefit from treatment with either DDR-targeting agents (e.g., PARP inhibitors or platinum) or cell cycle inhibitors (e.g., ATR and WEE1 inhibitors), our results demonstrate that FASN is a metabolic vulnerability that may confer sensitivity to therapeutics targeting the mitochondrial apoptotic machinery in this common subset of PDAC cells [82,83]. Nevertheless, the greatest efficacy of the combination of TVB FASNis with BH3 mimetics occurred in Mayo-4041 PDAC cells, a unique model of the classical (pancreatic) transcriptomic subtype that exhibits a high replication signature that is characteristic of the squamous (also referred to as quasi-mesenchymal or basal-like) molecular class of PDAC, further highlighting the therapeutic relevance of the FASNi/BH3 mimetics combo in the platinum-resistant setting [82].

Conclusions

Therapeutic resistance to standard cytotoxic therapies, including radiation and gemcitabine, is a hallmark of PDAC that is dependent, at least in part, on deregulation of the mitochondrial apoptotic machinery. Mitochondrial apoptotic priming, or how close a cell is to the threshold of apoptosis, is a critical determinant of whether a cancer cell will undergo apoptotic cell death following chemotherapy. Therefore, cancers that are highly primed are more chemosensitive, while chemoresistant tumors such as PDAC are poorly primed. Although strategies capable of elevating mitochondrial priming of PDAC cells could make PDAC cells more susceptible to killing, such a goal remains an unmet therapeutic challenge. Here, we demonstrate that the close interaction between lipogenic and mitochondrial apoptotic signaling pathways is a metabolic vulnerability that can be exploited to sensitize PDAC to BH3 mimetics (Fig. 6). TVB FASNis are a valuable family of metabolic drugs that

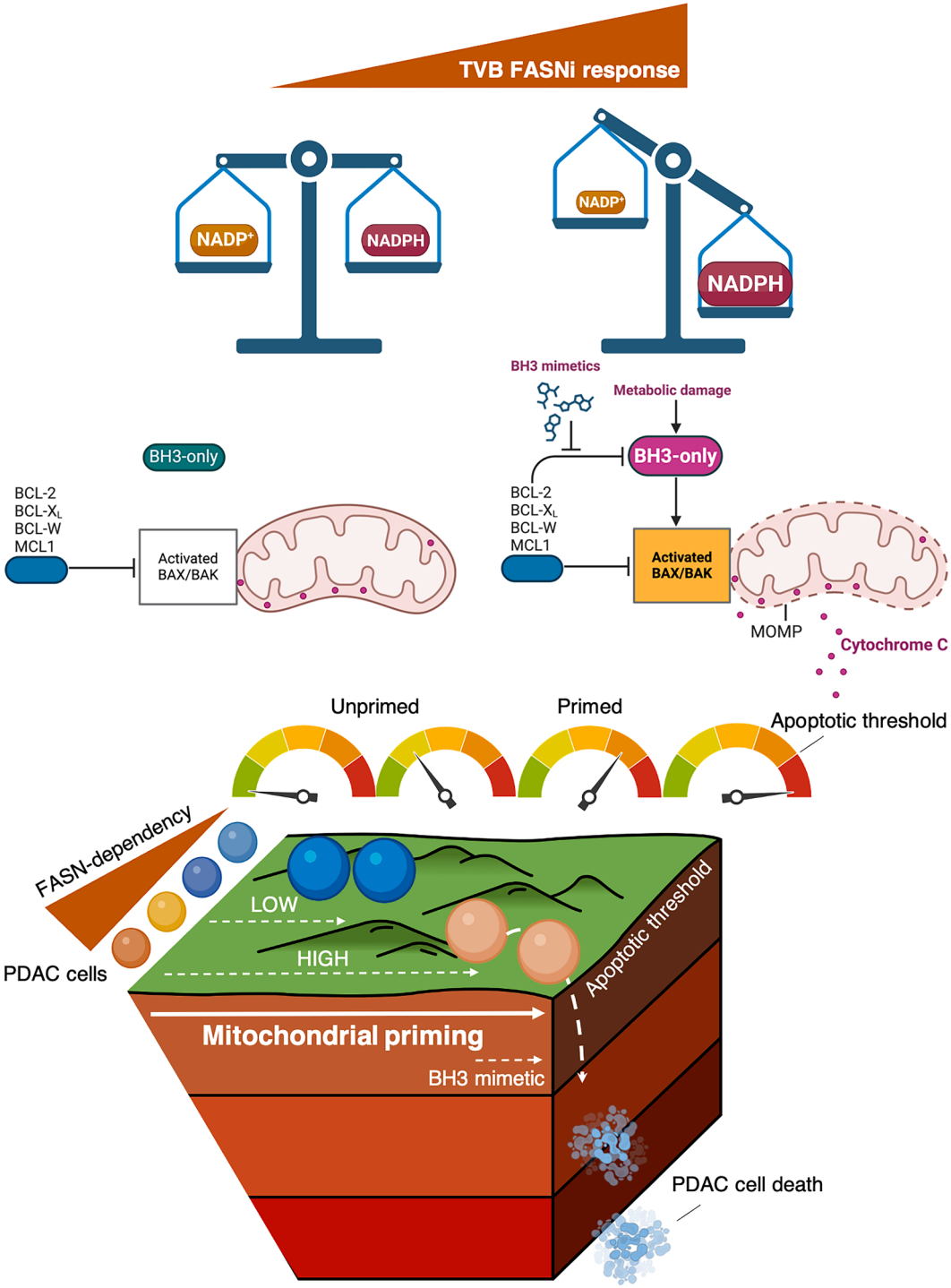

Fig. 6. FASN-regulated mitochondrial apoptotic priming: A therapeutic opportunity in PDAC. FASN inhibition increases the level of mitochondrial priming –the proximity to the apoptotic threshold represented here as the proximity to the "cliff edge"– in PDAC. The ability of highly primed PDAC cells to cross the apoptotic threshold and fall into the "senolytic Death Valley" can be readily enhanced in the presence of BH3 mimetics, which help to push FASNis-treated PDAC cells to the top of the cliff. FASNis and BH3 mimetics may show therapeutic efficacy against PDAC when used in combination due to both the dependence of PDAC on BCL-2 proteins for survival upon FASN blockade and the ability of BH3 mimetics to antagonize the pro-survival function of anti-apoptotic BCL-2 proteins. BH3 mimetics can fully unleash the intrinsic apoptotic pathway in FASN-inhibited PDAC cells primed for death, thereby revealing a critical vulnerability in the regulation of the mitochondrial apoptotic machinery downstream of FASN signaling (NADPH accumulation) that could transform the reversible tumor shrinkage seen with FASNis and BH3 mimetics as single agents into more complete and durable tumor regression when combined simultaneously.

specifically increase the antiapoptotic dependency of PDAC and consequently render PDAC cells highly sensitive to BH3 mimetics, which may warrant further preclinical exploration and possible clinical investigation in PDAC patients.

Abbreviations

AF2, AlphaFold2; Cryo-EM, Cryo-electron microscopy; DDR, DNA damage response; DPI, Diphenyleneiodonium; FASN, Fatty acid synthase; ASNi, FASN inhibitor; FOLFIRINOX, Fluorouracil, leucovorin,

irinotecan, and oxaliplatin; GSH, Reduced glutathione; NAC, N-acetyl cysteine; NADPH, Nicotinamide adenine dinucleotide phosphate; NOX, NADPH oxidase; PARP, Poly-ADP ribose polymerase; PDAC, Pancreatic ductal adenocarcinoma; PDX, Patient-derived xenograft; ROS, Reactive oxygen species

Funding

Work in the Ruth Lupu laboratory is supported by NIH National Cancer Institute Pancreatic Cancer SPORE Grant NCI P50 CA102701 and Developmental Research Program Pilot Projects and Awards from the Mayo Clinic Comprehensive Cancer Center provided by Dr. McWilliams. Work in the Javier A. Menendez laboratory is supported by the Ministerio de Ciencia e Innovación and the Spanish Research Agency (MCIN/AEI, grants PID2019-104055GB-I00 and PID2022-141955OB-I00 to Javier A. Menendez, Plan Nacional de I+D+i, funded by the European Regional Development Fund, "ERDF A way of making Europe"), and the Emerging Research Group SGR 2021 01507 of the Agència de Gestió d'Ajuts Universitaris i de Recerca (AGAUR, Generalitat de Catalunya). Dr. Kaufmann's work is partially supported uner NIH National Cancer Institute R01 CA225996. Elisabet Cuyàs holds a "Miguel Servet" research contract (CP20/00003) from the Instituto de Salud Carlos III (Spain) and is supported by the grant PI22/00297 (Instituto de Salud Carlos III, Proyectos de I+D+I en Salud, Acción Estratégica en Salud 2021–2023, funded by the "ERDF A way of making Europe"). Javier A. Menendez and Elisabet Cuyàs thank the CERCA Program/Generalitat de Catalunya for the institutional support of IDIBGI. Eila Serrano-Hervás holds an INVESTIGO research contract (2022 INV-1 00001, Next Generation Catalunya, Next Generation EU) from the Agència de Gestió d'Ajuts Universitaris i de Recerca (AGAUR, Generalitat de Catalunya). Cristina Duran was supported by a PhD fellowship from the Spanish MINECO (PRE2019-089147) and Guillem Casadevall by research grants from the ERC-StG (ERC-2015-StG-679001) and ERC-POC (ERC-2022-POC-101112805). Sílvia Osuna thanks the Generalitat de Catalunya for the consolidated group TCBioSys (SGR 2021 00487) and the Spanish Ministry of Science and Innovation (MCIN) for the grants PID2021-129034NB-I00 and PDC2022-133950-I00. Sílvia Osuna is grateful for funding from the European Research Council (ERC) under the European Union's Horizon 2020 research and innovation program (ERC-2022-POC-101112805, and ERC-2022-CoG-101088032), and the Human Frontier Science Program (HFSP) for project grant RGP0054/2020.

Data availability

The data in support of the findings of this study are available from the corresponding authors, upon reasonable request.

Ethics approval

Animal studies were conducted in accordance with the Guide for the Care and Use of Laboratory Animals and approved by Mayo Institutional Animal Care and Use Committee (IACUC) protocol A00001942-16-R22.

CRediT authorship contribution statement

Travis Vander Steen: Data curation, Formal analysis, Investigation, Methodology, Validation, Visualization. **Ingrid Espinoza:** Data curation, Formal analysis, Investigation, Methodology, Validation, Visualization. **Cristina Duran:** Data curation, Formal analysis, Investigation, Methodology, Validation, Visualization. **Guillem Casadevall:** Data curation, Formal analysis, Investigation, Methodology, Validation, Visualization. **Eila Serrano-Hervás:** Data curation, Formal analysis, Investigation, Methodology, Validation, Visualization. **Elisabet Cuyàs:** Data curation, Formal analysis, Validation, Visualization. **Sara Verdura:** Data curation, Formal analysis, Validation, Visualization. **George Kemble:** Conceptualization, Methodology, Resources. **Scott H. Kaufmann:** Conceptualization, Methodology, Resources, Writing – review & editing. **Robert McWilliams:** Conceptualization, Methodology, Resources, Writing – review & editing. **Sílvia Osuna:** Conceptualization, Methodology, Resources, Writing – review & editing. **Daniel D. Billadeau:** Conceptualization, Methodology, Resources, Writing – review & editing. **Javier A. Menendez:** Conceptualization, Funding acquisition, Methodology, Project administration, Resources, Supervision, Visualization, Writing – original draft, Writing – review & editing. **Ruth Lupu:** Conceptualization, Funding acquisition, Methodology, Project administration, Resources, Supervision, Visualization, Writing – original draft, Writing – review & editing.

Declaration of competing interest

George Kemble is the Chief Executive Officer and Chief Scientific Officer at Sagimet Biosciences (formerly known as 3-V Biosciences). All the other authors declare that the research was conducted in the absence of any commercial or financial relationship that could be construed as a potential conflict of interest. All authors consented to the publication of this article. All data were generated in-house and no paper mills were used. To ensure integrity and accuracy, all authors agree to take responsibility for all aspects of the work. The authors did not use any AI tool/service or AI-enabled technologies in the preparation of this paper.

Supplementary materials

Supplementary material associated with this article can be found, in the online version, at doi:10.1016/j.neo.2025.101143.

References

[1] L Rahib, BD Smith, R Aizenberg, AB Rosenzweig, JM Fleshman, LM. Matrisian, Projecting cancer incidence and deaths to 2030: the unexpected burden of thyroid, liver, and pancreas cancers in the United States, Cancer Res. 74 (2014) 2913–2921.
[2] JE Lim, MW Chien, CC. Earle, Prognostic factors following curative resection for pancreatic adenocarcinoma: a population-based, linked database analysis of 396 patients, Ann. Surg. 237 (2003) 74–85.
[3] KY Bilimoria, DJ Bentrem, CY Ko, JS Tomlinson, AK Stewart, DP Winchester, MS. Talamonti, Multimodality therapy for pancreatic cancer in the U.S.: utilization, outcomes, and the effect of hospital volume, Cancer 110 (2007) 1227–1234.
[4] M Wagner, C Redaelli, M Lietz, CA Seiler, H Friess, MW. Büchler, Curative resection is the single most important factor determining outcome in patients with pancreatic adenocarcinoma, Br. J. Surg. 91 (2004) 586–594.
[5] M. Hidalgo, Pancreatic cancer, N. Engl. J. Med. 362 (2010) 1605–1617.
[6] JP Neoptolemos, DD Stocken, H Friess, C Bassi, JA Dunn, H Hickey, H Beger, L Fernandez-Cruz, C Dervenis, F Lacaine, M Falconi, P Pederzoli, A Pap, D Spooner, DJ Kerr, MW Büchler, European Study Group for Pancreatic Cancer. A randomized trial of chemoradiotherapy and chemotherapy after resection of pancreatic cancer, N. Engl. J. Med. 350 (2004) 1200–1210.
[7] H Oettle, S Post, P Neuhaus, K Gellert, J Langrehr, K Ridwelski, H Schramm, J Fahlke, C Zuelke, C Burkart, K Gutberlet, E Kettner, H Schmalenberg, K Weigang-Koehler, WO Bechstein, M Niedergethmann, I Schmidt-Wolf, L Roll, B Doerken, H. Riess, Adjuvant chemotherapy with gemcitabine vs observation in patients undergoing curative-intent resection of pancreatic cancer: a randomized controlled trial, JAMA 297 (2007) 267–277.
[8] D Goldstein, RH El-Maraghi, P Hammel, V Heinemann, V Kunzmann, J Sastre, W Scheithauer, S Siena, J Tabernero, L Teixeira, G Tortora, JL Van Laethem, R Young, DN Penenberg, B Lu, A Romano, DD Von Hoff, nab-Paclitaxel plus gemcitabine for metastatic pancreatic cancer: long-term survival from a phase III trial, J. Natl. Cancer Inst. 107 (2015) dju413.
[9] R Petrioli, G Roviello, AI Fiaschi, L Laera, D Marrelli, F Roviello, E Francini, Gemcitabine, oxaliplatin, and capecitabine (GEMOXEL) compared with

gemcitabine alone in metastatic pancreatic cancer: a randomized phase II study, Cancer Chemother. Pharmacol. 75 (2015) 683–690.
[10] T Conroy, F Desseigne, M Ychou, O Bouché, R Guimbaud, Y Bécouarn, A Adenis, JL Raoul, S Gourgou-Bourgade, C de la Fouchardière, J Bennouna, JB Bachet, F Khemissa-Akouz, D Péré-Vergé, C Delbaldo, E Assenat, B Chauffert, P Michel, C Montoto-Grillot, M Ducreux, Groupe Tumeurs Digestives of Unicancer; PRODIGE Intergroup. FOLFIRINOX versus gemcitabine for metastatic pancreatic cancer, N. Engl. J. Med. 364 (2011) 1817–1825.
[11] DD Von Hoff, T Ervin, FP Arena, EG Chiorean, J Infante, M Moore, T Seay, SA Tjulandin, WW Ma, MN Saleh, M Harris, M Reni, S Dowden, D Laheru, N Bahary, RK Ramanathan, J Tabernero, M Hidalgo, D Goldstein, E Van Cutsem, X Wei, J Iglesias, MF Renschler, Increased survival in pancreatic cancer with nab-paclitaxel plus gemcitabine, N. Engl. J. Med. 369 (2013) 1691–1703.
[12] T Conroy, P Hammel, M Hebbar, Ben Abdelghani M, AC Wei, JL Raoul, L Choné, E Francois, P Artru, JJ Biagi, T Lecomte, E Assenat, R Faroux, M Ychou, J Volet, A Sauvanet, G Breysacher, Di Fiore F, C Cripps, P Kavan, P Texereau, K Bouhier-Leporrier, F Khemissa-Akouz, JL Legoux, B Juzyna, S Gourgou, CJ O'Callaghan, C Jouffroy-Zeller, P Rat, D Malka, F Castan, Bachet JB;, Canadian cancer trials group and the unicancer-GI–PRODIGE group. FOLFIRINOX or gemcitabine as adjuvant therapy for pancreatic cancer, N. Engl. J. Med. 379 (2018) 2395–2406.
[13] B Schniewind, M Christgen, R Kurdow, S Haye, B Kremer, H Kalthoff, H. Ungefroren, Resistance of pancreatic cancer to gemcitabine treatment is dependent on mitochondria-mediated apoptosis, Int. J. Cancer 109 (2004) 182–188.
[14] S Westphal, H. Kalthoff, Apoptosis: targets in pancreatic cancer, Mol. Cancer 2 (2003) 6.
[15] N Samm, K Werner, F Rückert, HD Saeger, R Grützmann, C. Pilarsky, The role of apoptosis in the pathology of pancreatic cancer, Cancers (Basel) 3 (2010) 1–16.
[16] A Arlt, SS Müerköster, H. Schäfer, Targeting apoptosis pathways in pancreatic cancer, Cancer Lett. 332 (2013) 346–358.
[17] Y Zhou, H Liu, R Xue, W Tang, S. Zhang, BH3 Mimetic ABT-199 Enhances the Sensitivity of Gemcitabine in Pancreatic Cancer in vitro and in vivo, Dig. Dis. Sci. 63 (2018) 3367–3375.
[18] Z Duan, D Chinn, MJ Tu, QY Zhang, J Huynh, J Chen, P Mack, AM Yu, EJ. Kim, Novel Synergistic Combination of Mitotic Arrest and Promotion of Apoptosis for Treatment of Pancreatic Adenocarcinoma, Transl. Oncol. 12 (2019) 68–392.
[19] BA Quinn, R Dash, S Sarkar, B Azab, P Bhoopathi, SK Das, L Emdad, J Wei, M Pellecchia, D Sarkar, PB. Fisher, Pancreatic Cancer Combination Therapy Using a BH3 Mimetic and a Synthetic Tetracycline, Cancer Res. 75 (2015) 2305–2315.
[20] S Kehr, M. Vogler, It's time to die: BH3 mimetics in solid tumors, Biochim. Biophys. Acta Mol. Cell Res. 1868 (2021) 118987.
[21] KA Sarosiek, T Ni Chonghaile, A Letai, Mitochondria: gatekeepers of response to chemotherapy, Trends Cell Biol. 23 (2013) 612–619.
[22] MS Cragg, C Harris, A Strasser, CL. Scott, Unleashing the power of inhibitors of oncogenic kinases through BH3 mimetics, Nat. Rev. Cancer 9 (2009) 321–326.
[23] KA Sarosiek, A. Letai, Directly targeting the mitochondrial pathway of apoptosis for cancer therapy using BH3 mimetics - recent successes, current challenges and future promise, FEBS J. 283 (2016) 3523–3533.
[24] A Ashkenazi, WJ Fairbrother, JD Leverson, AJ. Souers, From basic apoptosis discoveries to advanced selective BCL-2 family inhibitors, Nat. Rev. Drug Discov. 16 (2017) 273–284.
[25] J Montero, A. Letai, Why do BCL-2 inhibitors work and where should we use them in the clinic? Cell Death. Differ. 25 (2018) 56–64.
[26] ST Diepstraten, MA Anderson, PE Czabotar, G Lessene, A Strasser, GL. Kelly, The manipulation of apoptosis for cancer therapy using BH3-mimetic drugs, Nat. Rev. Cancer 22 (2022) 45–64.
[27] J Montero, R. Haq, Adapted to Survive: Targeting Cancer Cells with BH3 Mimetics, Cancer Discov. 12 (2022) 1217–1232.
[28] M Certo, V Del Gaizo Moore, M Nishino, G Wei, S Korsmeyer, SA Armstrong, A. Letai, Mitochondria primed by death signals determine cellular addiction to antiapoptotic BCL-2 family members, Cancer Cell 9 (2006) 351–365.
[29] V Del Gaizo Moore, A. Letai, BH3 profiling–measuring integrated function of the mitochondrial apoptotic pathway to predict cell fate decisions, Cancer Lett. 332 (2013) 202–205.
[30] M Butterworth, A Pettitt, S Varadarajan, GM. Cohen, BH3 profiling and a toolkit of BH3-mimetic drugs predict anti-apoptotic dependence of cancer cells, Br. J. Cancer 114 (2016) 638–641.
[31] M Villalobos-Ortiz, J Ryan, TN Mashaka, JT Opferman, A. Letai, BH3 profiling discriminates on-target small molecule BH3 mimetics from putative mimetics, Cell Death. Differ. 27 (2020) 999–1007.
[32] P Gomez-Bougie, S Maiga, B Tessoulin, J Bourcier, A Bonnet, MS Rodriguez, S Le Gouill, C Touzeau, P Moreau, C Pellat-Deceunynck, M Amiot, BH3-mimetic toolkit guides the respective use of BCL2 and MCL1 BH3-mimetics in myeloma treatment, Blood 132 (2018) 2656–2669.
[33] DS Potter, R Du, P Bhola, R Bueno, A. Letai, Dynamic BH3 profiling identifies active BH3 mimetic combinations in non-small cell lung cancer, Cell Death. Dis. 12 (2021) 741.
[34] T Ni Chonghaile, KA Sarosiek, TT Vo, JA Ryan, A Tammareddi, G Moore Vdel, J Deng, KC Anderson, P Richardson, YT Tai, CS Mitsiades, UA Matulonis, R Drapkin, R Stone, DJ Deangelo, DJ McConkey, SE Sallan, L Silverman, MS Hirsch, DR Carrasco, A Letai, Pretreatment mitochondrial priming correlates with clinical response to cytotoxic chemotherapy, Science 334 (2011) 1129–1133.
[35] J Montero, KA Sarosiek, JD DeAngelo, O Maertens, J Ryan, D Ercan, H Piao, NS Horowitz, RS Berkowitz, U Matulonis, PA Jänne, PC Amrein, K Cichowski, R Drapkin, A. Letai, Drug-induced death signaling strategy rapidly predicts cancer response to chemotherapy, Cell 160 (2015) 977–989.
[36] JS Garcia, S Bhatt, G Fell, AS Sperling, M Burgess, H Keshishian, B Yilma, A Brunner, D Neuberg, SA Carr, BL Ebert, K Ballen, RM Stone, DJ DeAngelo, BC Medeiros, A. Letai, Increased mitochondrial apoptotic priming with targeted therapy predicts clinical response to re-induction chemotherapy, Am. J. Hematol. 95 (2020) 245–250.
[37] P Paiva, FE Medina, M Viegas, P Ferreira, RPP Neves, JPM Sousa, MJ Ramos, PA. Fernandes, Animal fatty acid synthase: a chemical nanofactory, Chem. Rev. 121 (2021) 9502–9553.
[38] JA Menendez, R Lupu, Fatty acid synthase and the lipogenic phenotype in cancer pathogenesis, Nat. Rev. Cancer 7 (2007) 763–777.
[39] F Röhrig, A. Schulze, The multifaceted roles of fatty acid synthesis in cancer, Nat. Rev. Cancer 16 (2016) 732–749.
[40] N Koundouros, G. Poulogiannis, Reprogramming of fatty acid metabolism in cancer, Br. J. Cancer 122 (2020) 4–22.
[41] S Vasseur, F. Guillaumond, Lipids in cancer: a global view of the contribution of lipid pathways to metastatic formation and treatment resistance, Oncogenesis 11 (2022) 46.
[42] JA Menendez, E Cuyàs, JA Encinar, Vander Steen T, S Verdura, Llop-Hernández À, J López, E Serrano-Hervás, S Osuna, B Martin-Castillo, R Lupu, The fatty acid synthase (FASN) signalome: a molecular guide for precision oncology, Mol. Oncol. 18 (2024) 479–516.
[43] PL Alo, M Amini, F Piro, L Pizzuti, V Sebastiani, C Botti, R Murari, G Zotti, U. Di Tondo, Immunohistochemical expression and prognostic significance of fatty acid synthase in pancreatic carcinoma, Anticancer Res. 27 (2007) 2523–2527.
[44] AK Witkiewicz, KH Nguyen, A Dasgupta, EP Kennedy, CJ Yeo, MP Lisanti, JR. Brody, Co-expression of fatty acid synthase and caveolin-1 in pancreatic ductal adenocarcinoma: implications for tumor progression and clinical outcome, Cell Cycle 7 (2008) 3021–3025.
[45] K Walter, SM Hong, S Nyhan, M Canto, N Fedarko, A Klein, M Griffith, N Omura, S Medghalchi, F Kuhajda, M. Goggins, Serum fatty acid synthase as a marker of pancreatic neoplasia, Cancer Epidemiol. Biomarkers Prev. 18 (2009) 2380–2385.
[46] Y Yang, H Liu, Z Li, Z Zhao, M Yip-Schneider, Q Fan, CM Schmidt, EG Chiorean, J Xie, L Cheng, JH Chen, JT Zhang, Role of fatty acid synthase in gemcitabine and radiation resistance of pancreatic cancers, Int. J. Biochem. Mol. Biol. 2 (2011) 89–98.
[47] S Tadros, SK Shukla, RJ King, V Gunda, E Vernucci, J Abrego, NV Chaika, F Yu, AJ Lazenby, L Berim, J Grem, AR Sasson, PK Singh, *De Novo* Lipid Synthesis Facilitates Gemcitabine Resistance through Endoplasmic Reticulum Stress in Pancreatic Cancer, Cancer Res. 77 (2017) 5503–5517.
[48] S Tian, P Li, S Sheng, X Jin, Upregulation of pyruvate kinase M2 expression by fatty acid synthase contributes to gemcitabine resistance in pancreatic cancer, Oncol. Lett. 15 (2018) 2211–2217.
[49] G Falchook, J Infante, HT Arkenau, MR Patel, E Dean, E Borazanci, A Brenner, N Cook, J Lopez, S Pant, A Frankel, P Schmid, K Moore, W McCulloch, K Grimmer, M O'Farrell, G Kemble, H Burris, First-in-human study of the safety, pharmacokinetics, and pharmacodynamics of first-in-class fatty acid synthase inhibitor TVB-2640 alone and with a taxane in advanced tumors, EClinicalMedicine 34 (2021) 100797.
[50] R Loomba, R Mohseni, KJ Lucas, JA Gutierrez, RG Perry, JF Trotter, RS Rahimi, SA Harrison, V Ajmera, JD Wayne, M O'Farrell, W McCulloch, K Grimmer, M Rinella, Wong V Wai-Sun, V Ratziu, GJ Gores, BA Neuschwander-Tetri, G Kemble, TVB-2640 (FASN Inhibitor) for the treatment of nonalcoholic steatohepatitis: FASCINATE-1, a randomized, placebo-controlled phase 2a trial, Gastroenterology 161 (2021) 1475–1486.
[51] W Kelly, AE Diaz Duque, J Michalek, B Konkel, L Caflisch, Y Chen, SC Pathuri, V Madhusudanannair-Kunnuparampil, J Floyd, A. Brenner, Phase II investigation of TVB-2640 (Denifanstat) with bevacizumab in patients with first relapse high-grade astrocytoma, Clin. Cancer Res. 29 (2023) 2419–2425.
[52] B Schroeder, T Vander Steen, I Espinoza, CMK Venkatapoorna, Z Hu, FM Silva, K Regan, E Cuyàs, XW Meng, S Verdura, A Arbusà, PA Schneider, KS Flatten, G Kemble, J Montero, SH Kaufmann, JA Menendez, R Lupu, Fatty acid synthase (FASN) regulates the mitochondrial priming of cancer cells, Cell Death Dis. 12 (2021) 977.
[53] FP Kuhajda, ES Pizer, JN Li, NS Mani, GL Frehywot, CA. Townsend, Synthesis and antitumor activity of an inhibitor of fatty acid synthase, Proc. Natl. Acad. Sci. U.S. A. 97 (2000) 3450–3454.
[54] K Makowski, P Mera, D Paredes, L Herrero, X Ariza, G Asins, FG Hegardt, J García, D. Serra, Differential pharmacologic properties of the two C75 enantiomers: (+)-C75 is a strong anorectic drug; (-)-C75 has antitumor activity, Chirality 25 (2013) 281–287.
[55] JA Menendez, R. Lupu, Fatty acid synthase (FASN) as a therapeutic target in breast cancer, Expert Opin. Ther. Targets 21 (2017) 1001–1016.
[56] N Montesdeoca, M López, X Ariza, L Herrero, K. Makowski, Inhibitors of lipogenic enzymes as a potential therapy against cancer, FASEB J. 34 (2020) 11355–11381.
[57] DS Potter, A. Letai, To prime, or not to prime: that is the question, Cold. Spring. Harb. Symp. Quant. Biol. 81 (2016) 131–140.
[58] T Kuehl, D. Lagares, BH3 mimetics as anti-fibrotic therapy: Unleashing the mitochondrial pathway of apoptosis in myofibroblasts, Matrix. Biol. 68-69 (2018) 94–105.
[59] B Hinz, D. Lagares, Evasion of apoptosis by myofibroblasts: a hallmark of fibrotic diseases, Nat. Rev. Rheumatol. 16 (2020) 11–31.
[60] JE Guikema, M Amiot, E. Eldering, Exploiting the pro-apoptotic function of NOXA as a therapeutic modality in cancer, Expert Opin. Ther. Targets 21 (2017) 767–779.

[61] EL Britt, S Raman, K Leek, CH Sheehy, SW Kim, H. Harada, Combination of fenretinide and ABT-263 induces apoptosis through NOXA for head and neck squamous cell carcinoma treatment, PLoS One 14 (2019) e0219398.

[62] TM Loftus, DE Jaworsky, GL Frehywot, CA Townsend, GV Ronnett, MD Lane, FP. Kuhajda, Reduced food intake and body weight in mice treated with fatty acid synthase inhibitors, Science 288 (2000) 2379–2381.

[63] JN Thupari, LE Landree, GV Ronnett, FP. Kuhajda, C75 increases peripheral energy utilization and fatty acid oxidation in diet-induced obesity, Proc. Natl. Acad. Sci. U.S.A. 99 (2002) 9498–9502.

[64] R Ventura, K Mordec, J Waszczuk, Z Wang, J Lai, M Fridlib, D Buckley, G Kemble, TS. Heuer, Inhibition of de novo palmitate synthesis by fatty acid synthase induces apoptosis in tumor cells by remodeling cell membranes, inhibiting signaling pathways, and reprogramming gene expression, EBioMedicine 2 (2015) 808–824.

[65] TS Heuer, R Ventura, K Mordec, J Lai, M Fridlib, D Buckley, G. Kemble, FASN inhibition and taxane treatment combine to enhance anti-tumor efficacy in diverse xenograft tumor models through disruption of tubulin palmitoylation and microtubule organization and FASN inhibition-mediated effects on oncogenic signaling and gene expression, EBioMedicine 16 (2017) 51–62.

[66] SMN Hasan, JW Lou, AFA Keszei, DL Dai, MT Mazhab-Jafari, Atomic model for core modifying region of human fatty acid synthase in complex with Denifanstat, Nat. Commun. 14 (2023) 3460.

[67] MA Hardwicke, AR Rendina, SP Williams, ML Moore, L Wang, JA Krueger, RN Plant, RD Totoritis, G Zhang, J Briand, WA Burkhart, KK Brown, CA. Parrish, A human fatty acid synthase inhibitor binds β-ketoacyl reductase in the keto-substrate site, Nat. Chem. Biol. 10 (2014) 774–779.

[68] JK Brunelle, A. Letai, Control of mitochondrial apoptosis by the Bcl-2 family, J. Cell Sci. 122 (2009) 437–441.

[69] H Kalkavan, DR. Green, MOMP, cell suicide as a BCL-2 family business, Cell Death Differ. 25 (2018) 46–55.

[70] M Zafarullah, WQ Li, J Sylvester, M. Ahmad, Molecular mechanisms of N-acetylcysteine actions, Cell Mol. Life Sci. 60 (2003) 6–20.

[71] K Shimamoto, H Hayashi, E Taniai, R Morita, M Imaoka, Y Ishii, et al., Antioxidant N-acetyl-L-cysteine (NAC) supplementation reduces reactive oxygen species (ROS)-mediated hepatocellular tumor promotion of indole-3-carbinol (I3C) in rats, J. Toxicol. Sci. 36 (2011) 775–786.

[72] Y Li, MA. Trush, Diphenyleneiodonium, an NAD(P)H oxidase inhibitor, also potently inhibits mitochondrial reactive oxygen species production, Biochem. Biophys. Res. Commun. 253 (1998) 295–299.

[73] C Riganti, E Gazzano, M Polimeni, C Costamagna, A Bosia, D. Ghigo, Diphenyleneiodonium inhibits the cell redox metabolism and induces oxidative stress, J. Biol. Chem. 279 (2004) 47726–47731.

[74] HQ Ju, JF Lin, T Tian, D Xie, RH. Xu, NADPH homeostasis in cancer: functions, mechanisms and therapeutic implications, Signal. Transduct. Target. Ther. 5 (2020) 231.

[75] Y Cui, P Xing, Y Wang, M Liu, L Qiu, G Ying, B Li, NADPH accumulation is responsible for apoptosis in breast cancer cells induced by fatty acid synthase inhibition, Oncotarget 8 (2017) 32576–32585.

[76] J Cheng, KJ Okolotowicz, D Ryan, E Mose, AM Lowy, JR Cashman, Inhibition of invasive pancreatic cancer: restoring cell apoptosis by activating mitochondrial p53, Am. J. Cancer Res. 9 (2019) 390–405.

[77] H Masuo, K Kubota, A Shimizu, T Notake, S Miyazaki, T Yoshizawa, H Sakai, H Hayashi, Y. Soejima, Increased mitochondria are responsible for the acquisition of gemcitabine resistance in pancreatic cancer cell lines, Cancer Sci. 114 (2023) 4388–4400.

[78] D Thummuri, S Khan, PW Underwood, P Zhang, J Wiegand, X Zhang, V Budamagunta, A Sobh, A Tagmount, A Loguinov, AN Riner, AS Akki, E Williamson, R Hromas, CD Vulpe, G Zheng, JG Trevino, D. Zhou, Overcoming gemcitabine resistance in pancreatic cancer using the BCL-X_L-specific degrader DT2216, Mol. Cancer Ther. 21 (2022) 184–192.

[79] J Jung, CH Lee, HS Seol, YS Choi, E Kim, EJ Lee, JK Rhee, SR Singh, ES Jun, B Han, SM Hong, SC Kim, S. Chang, Generation and molecular characterization of pancreatic cancer patient-derived xenografts reveals their heterologous nature, Oncotarget 7 (2016) 62533–62546.

[80] ES Knudsen, U Balaji, B Mannakee, P Vail, C Eslinger, C Moxom, J Mansour, AK. Witkiewicz, Pancreatic cancer cell lines as patient-derived avatars: genetic characterisation and functional utility, Gut 67 (2018) 508–520.

[81] PL Garcia, AL Miller, KJ. Yoon, Patient-derived xenograft models of pancreatic cancer: overview and comparison with other types of models, Cancers (Basel) 12 (2020) 1327.

[82] Dreyer SB, Upstill-Goddard R, Paulus-Hock V, Paris C, Lampraki EM, Dray E, Serrels B, Caligiuri G, Rebus S, Plenker D, Galluzzo Z, Brunton H, Cunningham R, Tesson M, Nourse C, Bailey UM, Jones M, Moran-Jones K, Wright DW, Duthie F, Oien K, Evers L, McKay CJ, McGregor GA, Gulati A, Brough R, Bajrami I, Pettitt S, Dziubinski ML, Candido J, Balkwill F, Barry ST, Grützmann R, Rahib L; Glasgow Precision Oncology Laboratory; Australian Pancreatic Cancer Genome Initiative; Johns A, Pajic M, Froeling FEM, Beer P, Musgrove EA, Petersen GM, Ashworth A, Frame MC, Crawford HC, Simeone DM, Lord C, Mukhopadhyay D, Pilarsky C, Tuveson DA, Cooke SL, Jamieson NB, Morton JP, Sansom OJ, Bailey PJ, Biankin AV, Chang DK. Targeting DNA damage response and replication stress in pancreatic cancer. Gastroenterology. 2021;160:362–77.e13.

[83] P Bailey, DK Chang, K Nones, AL Johns, AM Patch, MC Gingras, DK Miller, AN Christ, TJ Bruxner, MC Quinn, C Nourse, LC Murtaugh, I Harliwong, S Idrisoglu, S Manning, E Nourbakhsh, S Wani, L Fink, O Holmes, V Chin, MJ Anderson, S Kazakoff, C Leonard, F Newell, N Waddell, S Wood, Q Xu, PJ Wilson, N Cloonan, KS Kassahn, D Taylor, K Quek, A Robertson, L Pantano, L Mincarelli, LN Sanchez, L Evers, J Wu, M Pinese, MJ Cowley, MD Jones, EK Colvin, AM Nagrial, ES Humphrey, LA Chantrill, A Mawson, J Humphris, A Chou, M Pajic, CJ Scarlett, AV Pinho, M Giry-Laterriere, I Rooman, JS Samra, JG Kench, JA Lovell, ND Merrett, CW Toon, K Epari, NQ Nguyen, A Barbour, N Zeps, K Moran-Jones, NB Jamieson, JS Graham, F Duthie, K Oien, J Hair, R Grützmann, A Maitra, CA Iacobuzio-Donahue, CL Wolfgang, RA Morgan, RT Lawlor, V Corbo, C Bassi, B Rusev, P Capelli, R Salvia, G Tortora, D Mukhopadhyay, GM Petersen, Australian Pancreatic Cancer Genome Initiative, DM Munzy, WE Fisher, SA Karim, JR Eshleman, RH Hruban, C Pilarsky, JP Morton, OJ Sansom, A Scarpa, EA Musgrove, UM Bailey, O Hofmann, RL Sutherland, DA Wheeler, AJ Gill, RA Gibbs, JV Pearson, N Waddell, AV Biankin, SM. Grimmond, Genomic analyses identify molecular subtypes of pancreatic cancer, Nature 531 (2016) 47–52.

[84] EA Collisson, P Bailey, DK Chang, AV Biankin, Molecular subtypes of pancreatic cancer, Nat. Rev. Gastroenterol. Hepatol. 16 (2019) 207–220.

[85] G Sagar, RP Sah, N Javeed, SK Dutta, TC Smyrk, JS Lau, N Giorgadze, T Tchkonia, JL Kirkland, ST Chari, D. Mukhopadhyay, Pathogenesis of pancreatic cancer exosome-induced lipolysis in adipose tissue, Gut 65 (2016) 1165–1174.

[86] L Ding, VS Madamsetty, S Kiers, O Alekhina, A Ugolkov, J Dube, Y Zhang, JS Zhang, E Wang, SK Dutta, DM Schmitt, FJ Giles, AP Kozikowski, AP Mazar, D Mukhopadhyay, DD. Billadeau, Glycogen synthase kinase-3 inhibition sensitizes pancreatic cancer cells to chemotherapy by abrogating the TopBP1/ATR-mediated DNA damage Response, Clin. Cancer Res. 25 (2019) 6452–6462.

[87] R Gogada, N Yadav, J Liu, S Tang, D Zhang, A Schneider, A Seshadri, L Sun, CM Aldaz, DG Tang, D. Chandra, Bim, a proapoptotic protein, up-regulated via transcription factor E2F1-dependent mechanism, functions as a prosurvival molecule in cancer, J. Biol. Chem. 288 (2013) 368–381.

[88] K Nakano, KH. Vousden, PUMA, a novel proapoptotic gene, is induced by p53, Mol. Cell 7 (2001) 683–694.

[89] E Oda, R Ohki, H Murasawa, J Nemoto, T Shibue, T Yamashita, T Tokino, T Taniguchi, N. Tanaka, Noxa, a BH3-only member of the Bcl-2 family and candidate mediator of p53-induced apoptosis, Science 288 (2000) 1053–1058.

[90] MJ Bueno, V Jimenez-Renard, S Samino, J Capellades, A Junza, ML López-Rodríguez, J Garcia-Carceles, I Lopez-Fabuel, JP Bolaños, NS Chandel, O Yanes, R Colomer, M. Quintela-Fandino, Essentiality of fatty acid synthase in the 2D to anchorage-independent growth transition in transforming cells, Nat. Commun. 10 (2019) 5011.

[91] F Magnani, A Mattevi, Structure and mechanisms of ROS generation by NADPH oxidases, Curr. Opin. Struct. Biol. 59 (2019) 91–97.

[92] A Vermot, I Petit-Härtlein, SME Smith, F Fieschi, NADPH oxidases (NOX): an overview from discovery, Mol. Mech. Physiol. Pathol. Antioxidants (Basel). 10 (2021) 890.

[93] A Cipriano, M Viviano, A Feoli, C Milite, G Sarno, S Castellano, G. Sbardella, NADPH Oxidases: from molecular mechanisms to current inhibitors, J. Med. Chem. 66 (2023) 11632–11655.

[94] Q Yu, CF Lee, W Wang, G Karamanlidis, J Kuroda, S Matsushima, J Sadoshima, R. Tian, Elimination of NADPH oxidase activity promotes reductive stress and sensitizes the heart to ischemic injury, J. Am. Heart. Assoc. 3 (2014) e000555.

[95] W Xiao, RS Wang, DE Handy, J Loscalzo, NAD(H) and NADP(H) redox couples and cellular energy metabolism, Antioxid. Redox Signal 28 (2018) 251–272.

[96] W Xiao, J Loscalzo, Metabolic responses to reductive stress, Antioxid. Redox. Signal 32 (2020) 1330–1337.

[97] KS Chun, DH Kim, YJ. Surh, Role of reductive versus oxidative stress in tumor progression and anticancer drug resistance, Cells 10 (2021) 758.

[98] MH Elbatreek, H Mucke, HHHW. Schmidt, NOX Inhibitors: from bench to Naxibs to bedside, Handb. Exp. Pharmacol. 264 (2021) 145–168.

[99] S Altenhöfer, KA Radermacher, PW Kleikers, K Wingler, HH. Schmidt, Evolution of NADPH oxidase inhibitors: selectivity and mechanisms for target engagement, Antioxid. Redox Signal 23 (2015) 406–427.

[100] VW Daniels, JJ Zoeller, N van Gastel, KE McQueeney, S Parvin, DS Potter, GG Fell, VG Ferreira, B Yilma, R Gupta, J Spetz, PD Bhola, JE Endress, IS Harris, E Carrilho, KA Sarosiek, DT Scadden, JS Brugge, A. Letai, Metabolic perturbations sensitize triple-negative breast cancers to apoptosis induced by BH3 mimetics, Sci. Signal. 14 (2021) eabc7405.

[101] R Hamacher, RM Schmid, D Saur, G Schneider, Apoptotic pathways in pancreatic ductal adenocarcinoma, Mol. Cancer 7 (2008) 64.

[102] W Nakajima, MA Hicks, N Tanaka, GW Krystal, H. Harada, Noxa determines localization and stability of MCL-1 and consequently ABT-737 sensitivity in small cell lung cancer, Cell Death Dis. 5 (2014) e1052.

[103] EL Britt, S Raman, K Leek, CH Sheehy, SW Kim, H. Harada, Combination of fenretinide and ABT-263 induces apoptosis through NOXA for head and neck squamous cell carcinoma treatment, PLoS One 14 (2019) e0219398.

[104] K Ohgino, H Terai, H Yasuda, S Nukaga, J Hamamoto, T Tani, A Kuroda, D Arai, K Ishioka, K Masuzawa, S Ikemura, I Kawada, K Naoki, K Fukunaga, K. Soejima, Intracellular levels of reactive oxygen species correlate with ABT-263 sensitivity in non-small-cell lung cancer cells, Cancer Sci. 111 (2020) 3793–3801.

[105] K Pal, AA Pletnev, SK Dutta, E Wang, R Zhao, A Baral, VK Yadav, S Aggarwal, S Krishnaswamy, KM Alkharfy, S Chowdhury, MR Spaller, D. Mukhopadhyay, Inhibition of endoglin-GIPC interaction inhibits pancreatic cancer cell growth, Mol. Cancer Ther. 13 (2014) 2264–2275.

[106] K Tunyasuvunakool, J Adler, Z Wu, T Green, M Zielinski, A Žídek, A Bridgland, A Cowie, C Meyer, A Laydon, S Velankar, GJ Kleywegt, A Bateman, R Evans, A Pritzel, M Figurnov, O Ronneberger, R Bates, SAA Kohl, A Potapenko, AJ Ballard, B Romera-Paredes, S Nikolov, R Jain, E Clancy, D Reiman, S Petersen, AW Senior, K Kavukcuoglu, E Birney, P Kohli, J Jumper, D. Hassabis, Highly

accurate protein structure prediction for the human proteome, Nature 596 (2021) 590–596.
[107] C Dominguez, R Boelens, AM. Bonvin, HADDOCK: a protein-protein docking approach based on biochemical or biophysical information, J. Am. Chem. Soc. 125 (2003) 1731–1737.
[108] GCP van Zundert, JPGLM Rodrigues, M Trellet, C Schmitz, PL Kastritis, E Karaca, ASJ Melquiond, M van Dijk, SJ de Vries, AMJJ. Bonvin, The HADDOCK2.2 Web server: user-friendly integrative modeling of biomolecular complexes, J. Mol. Biol. 428 (2016) 720–725.
[109] S Grimme, S Ehrlich, L Goerigk, Effect of the damping function in dispersion corrected density functional theory, J. Comput. Chem. 32 (2011) 1456–1465.
[110] S Zhao, H Wei, P Cieplak, Y Duan, R. Luo, *PyRESP*: a program for electrostatic parameterizations of additive and induced dipole polarizable force fields, J. Chem. Theory. Comput. 18 (2022) 3654–3670.
[111] AW Sousa da Silva, WF. Vranken, ACPYPE - AnteChamber PYthon parser interfacE, BMC. Res. Notes. 5 (2012) 367.